ABSTRACT

Title of Thesis: A STUDY OF THE FIRE DYNAMICS SIMULATOR (FDS)- CREATING LIFE-LIKE MOVIES AND STUDYING THE ACCURACY OF THE LAGRANGIAN PARTICLE MODEL

Zishanul Haque Hussain, Master of Science, 2023

Thesis Directed By: Dr. Arnaud Trouve, Fire Protection Engineering

Fire Dynamic Simulator (FDS) is a computational fluid dynamics (CFD) model of fire-driven fluid flow. It was first released publicly in February 2000[1].

Using SmokeView or Pyrosim to view the results of FDS simulations provides a powerful non-immersive virtual reality experience. It can be used in fire engineering, fire safety training, and fire investigation. By providing a more engaging and interactive user experience, non-immersive VR can help improve understanding and develop effective fire safety and prevention strategies.

On the other hand, FDS is a powerful tool for modeling the physics of fire behavior in buildings and other structures. It has been shown to produce accurate descriptions of fire behavior under a variety of different conditions.

This study touches on very divergent, yet very critical, aspects of the applications of FDS.

First, generating life-like simulations of fire and smoke characterized by different growth rates and surroundings (a non-immersive virtual reality application). Human behaviour experiments at Morgan State University will use the simulation videos to assess the accuracy of human estimates of fire growth rates and understand how situational factors impact human response.

The second part of the study focuses on the Lagrangian particle representation of water droplets in FDS simulations of fire suppression. This study id is going to look at the fire suppression model in which fire suppression is defined by surface wetting or the mass of water falling in the fire surface. The Lagrangian liquid water droplets tracked by FDS represent a larger number of actual droplets. The number of ‘super drops’ can affect the accuracy of the simulations. The particle insertion rate has a default value and controls the mass of the 'super drop'. FDS allows altering the particle insertion rate and hence the mass of the 'super drop. The goal is to find out how changing particle injection rate and mesh grid size impacts the accuracy of the simulation of water sprays.

A STUDY OF THE FIRE DYNAMICS SIMULATOR (FDS)- CREATING LIFE-LIKE MOVIES AND STUDYING THE ACCURACY OF THE LAGRANGIAN PARTICLE MODEL

by

Zishanul Haque Hussain

Thesis submitted to the Faculty of the Graduate School of the
University of Maryland, College Park, in partial fulfillment
of the requirements for the degree of
Master of Science
2023

Advisory Committee:
Professor Arnaud Trouve, Chair
Dr. James Milke
Dr. Peter Sunderland

© Copyright by
Zishanul Haque Hussain
2023

Dedication

To my beautiful wife, Shireen.
Thank you for everything.
This would not have been possible without your love and support.
And
To my wonderful daughter, Ariana.
You made it more exciting.

Acknowledgements

I am incredibly grateful to Dr. Arnaud Trouve for considering me to be a suitable candidate for the research project. Without his unwavering support, I would not have been able to achieve this accomplishment. His vast knowledge in the subject matter has been a guiding force throughout the entire journey. His insights and recommendations have been invaluable in helping me navigate the complexities of the research process.

In addition to Dr. Trouve's support, I would also like to express my sincere appreciation to the Department of Fire Protection Engineering for providing me with the positions of Research Assistant and Teaching Assistant. These positions have allowed me to pursue my education while also gaining valuable hands-on experience.

I would also like to acknowledge the contributions of Dr. Jim Milke, whose expertise in the fields of human behavior and smoke engineering have been incredibly beneficial to the research project. His guidance and support have been instrumental in shaping my understanding of the subject matter.

Finally, I would like to extend my gratitude to Dr. Justin Bonny at the Morgan State University for providing me with clear direction and guidance. His insights and recommendations have been invaluable in helping me to better understand the requirements of the project and to stay on track throughout its execution.

Table of Contents

Dedication ii

Acknowledgements iii

Table of Contents iv

List of Tables vi

List of Figures vii

List of Abbreviations ix

Chapter 1: Introduction- National Science Foundation Project 1

1.1 Background 1

1.1 Objective 3
1.3 Pyrosim 4
Chapter 2: The Model 5

2.1 Simulations 5
2.2 Material of Reaction 5
2.3 Heat Release Rate 6
2.4 RAMP & SPREAD_RATE 8
2.5 Simulation Time 11
2.6 The Computational Domain 12
2.5 Fuel Source 12
Chapter 3: Data Collection 14

3.1 Point of View 14
..... 14
3.2 DEVC & SLCF 16
Chapter 4: Resolution 18

4.1 Mesh size 18
4.2 Computation Time 19
4.3 Frames per second 19
4.4 Fire Simulation for Response Assesment 20
Chapter 5: Conclusion – NSF Project 22

Chapter 6: Introduction- The Lagrangian Model Project 23

6.1 Background 23

6.2 Hypothesis 24
Chapter 7: The Computation Domain 26

7.1 The Setting 26
7.2 Grid Sizes 26
7.3 Paticle Injection Characteristics and Rate 28
7.4 Simulation Time 30
7.5 Location of Slice 30
Chapter 8: Analysis 31

8.1 Mass Conservation 31
8.2 Reading the Slice Files 33
8.3 Mean Mass Flux 34
..... 36
8.4 Variability in Mass Flux 36
Chapter 9: Revisiting the Hypothesis 41

..... 43
Chapter 10: Simulation with a Fire 47

10.1 Analysis with Fire 47
10.2 Analysing with 'e_coefficient' 52
Chapter 11: Conclusion- Particles Project 55

11.1 Conclusion 55
11.2 Future Work 56
Appendix A: Using RAMP in FDS 57

Appendix B: Using SPREAD_RATE in FDS 61

Appendix C: Alternate Method to Place Observer 62

Appendix D: Using 'slread.m' to Read Slice Files 64

Bibliography 65

List of Tables

Table 1: Combustion properties of GM27 Polyurethane, borrowed from Table A.38 and A.39 of the SFPE Handbook of Fire Protection Engineering (2016 edition). 6
Table 2: shows the times required of different types of growths and the corresponding ‘α’s. 7
Table 3: Calculation for an average height of eye base on CDC data. 15
Table 4: CPU times 19

List of Figures

Figure 1: Comparison of visuals at different stages in a growing fire. Top: Shot at 13 seconds in a fire growing at a 'Warp' rate. Bottom: Shot at 29 second a fire growing at a 'Warp' rate. 3
Figure 2: Heat Release rate vs time for different categories of growth rates. 7
Figure 3: Heat Release rate vs time for simulated example (see Appendix A) for an ultra-fast growth rate fire. 8
Figure 4: Heat Release rate vs time for simulated example using RAMP and SPREAD_RATE..... 11
Figure 5: Different types of room configurations. Top left: Bedroom, Top Right: Kitchen, Bottom Left: Living Room, Bottom Right: Office. 13
Figure 6: Location of observers (Yellow dots), Green text represents the description of the device. 14
Figure 7: Height of observer. 15
Figure 8: A typical view of fire obstruction from the point of view near the door. .. 16
Figure 9: Visibility vs time for warp growth rate in bedroom setup. 17
Figure 10: Comparison between 5 cm and 2.5 cm grid cells. Left: 5 cm grid cells, Right: 2.5 cm grid cells. 18
Figure 11: Fire from a point of view of an observer; Top left: Bedroom, Top Right: Living Room, Bottom Left: Kitchen, Bottom Right: Office. 20
Figure 12: Top Left: Setup with no fire. Top Right: Setup with fire below the nozzle. Bottom Left: Setup with fire offset from the center of the nozzle..... 27
Figure 13: Top Left: 0.1m cells. Top Right: 0.2m cells. Bottom Left: 0.4m cells 27
Figure 14: 5000 Particles/s without a fire. 29
Figure 15: 5000 Particles/s with a fire below the nozzle. 29
Figure 16: 5000 Particles/s with a fire offset from the center of the nozzle. 30
Figure 17: Location of devices in the computational domain to check the conservation of mass. 32
Figure 18: Mass conservation using 'PARTICLE FLUZ Z' 32
Figure 19: Mass conservation using 'AMPUA' 33
Figure 20: A slice file at Z=0.1m showing the water mass flux in the Z direction ... 34
Figure 21: A slice showing the mean particle mass particle mass flux at Z = 0.1..... 35
Figure 22: A slice showing the mean particle mass flux at Z=0.1 meters with the line of cells considered for analysis shown in yellow..... 36
Figure 23: Comparison of mean of particle mass flux with varying particle injection rates and a 0.4 meter grid cell configuration..... 38
Figure 24: Comparison of Sample Standard Deviation of particle mass flux with varying particle injection rates in a 0.4 meter grid cell configuration 38
Figure 25: Comparison of mean of particle mass flux with a fixed particle injection rate (at 5000 particles/s) in different grid cell configurations..... 39
Figure 26: Comparison of mean of particle mass flux with a fixed particle injection rate (at 5000 particles/s) in different grid cell configurations..... 40
Figure 27: Comparison of mean of particle mass flux with particle injection rate for different choices of grid resolution. 40

Figure 28: Location of the cell at X=0.25m, Y=5m 41
Figure 29: Time variations of the mass flux of particles passing through a single cell of 0.1 meter size. 42
Figure 30: Time variations of the mass flux of particles passing through a single cell of 0.2 meter size. 42
Figure 31: Time variations of the mass flux of particles passing through a single cell of 0.4 meter size. 43
Figure 32: Comparison of the number of instances when no particle passes through the cell with different cell sizes. 43
Figure 33: Time variations of the mass flux of particles passing through a single cell of 0.4 meter size at 3000 particle/s. 44
Figure 34: Time variations of the mass flux of particles passing through a single cell of 0.4 meter size at 9000 particle/s. 45
Figure 35: Time variations of the mass flux of particles passing through a single cell of 0.4 meter size at 30000 particle/s. 45
Figure 36: Comparison of the number of instances when no particle passes through the cell with different particle insertion rates. 46
Figure 37: Heat release rate for simulations with fire. 47
Figure 38: Average Sample Standard Deviation of 3000 particle/s with 0.4 meters cell size compared to the values without fire data 48
Figure 39: Average Sample Standard Deviation of 9000 particle/s with 0.2 meters cell size compared to the values without fire data. 48
Figure 40: Average Sample Standard Deviation of 30000 particle/s with 0.1 meters cell size compared to the values without fire data. 49
Figure 41: Comparison of the mean of particle flux without fire and with fire at the center. 50
Figure 42: Comparison of the mean of particle flux without fire and with fire at the center. 50
Figure 43: Comparison of the mean of particle flux without fire and with offset fire. 51
Figure 44: Comparison of Sample Standard Deviation of particle flux without fire and with offset fire. 51
Figure 45: Comparison of the time variations of the heat release rate for different values of the particle injection rate. 53
Figure 46: Comparison of the time variations of the heat release rate for different values of the particle injection rate. 54

List of Abbreviations

ASET	Available Safe Egress Time
RSET	Required Safety Egress Time
FDS	Fire Dynamics Simulator
NIST	National Institute of Standards and Technology
VR	Virtual Reality
GUI	Graphical User Interface
HPC	High-performance Computing
HRR	Heat Release Rate
CDC	Centers for Disease Control and Pevention
CPU	Central Processing Unit

Chapter 1: Introduction- National Science Foundation Project

1.1 Background

Performance-based design in life safety problems essentially requires the estimation of Available Safe Egress Time (ASET) and Required Safety Egress Time (RSET). The RSET has two major components; the pre-movement and movement-time[2]. With the development of more advanced and sophisticated computer modelling tools, the accuracy of prediction of movement time, based on the surrounding space and occupant load, can be done very accurately. However, more research is needed to incorporate the behavioural aspect into estimating the pre-movement time[3]. A deeper understanding of the impact of human behaviour on pre-movement time will improve the current RSET prediction models.

Visual characteristics of smoke and flames can serve as indicators of the growth rate and intensity (generally quantified by Heat Release Rate) of fires. These include the density of smoke, the height of the smoke layer, the height and width of the flames, the color of the flames, and the flicker of flames[4]. Figure 1 shows the snapshots of a flame at two different stages of a growing fire. Just looking at the flame and smoke, one can clearly tell that the fire in the second snap has a higher intensity.

As the fire cues change over time during developing fires, the accuracy of detecting these changes could aid in evacuating during fires in a timely manner. Studies suggest that occupants use both the presence of fire cues and the intensity of such cues to decide the actions that they take[5,6].

Situational factors, such as the type of room and location of the occupant in relation to the fire, can impact pre-movement decision-making[7]; One could ignore visible smoke coming out from the kitchen. Occupants are more likely to take protective action when they are located in close proximity or within line of sight of the fire[8].

Combining fire dynamics simulations (FDS) with non-immersive virtual reality (VR) technology can create interactive visualizations that serve as effective tools for fire safety training and evacuation guidance[9,10]. Additionally, this combination can provide valuable insights into human behavior during pre-movement time.

Non-immersive VR technology offers a 3D visual representation of a simulated fire scenario, enabling users to experience and interact with the simulation in a safe and controlled environment. This technology can be utilized to create interactive visualizations of FDS simulations and further our understanding of how humans perceive visual cues through experimentation.

Overall, the integration of FDS, non-immersive VR technology, and research on human behavior can enhance fire safety training and evacuation guidance, leading to better preparation and response during emergency situations.

The aim of this study is to develop a library of simulations of fires that can be used for non-immersive virtual reality during human behaviour experiments:

a. To assess the accuracy of human estimates of growth rates.
b. Identify how situational factors enhance or reduce the accuracy of fire growth rate estimates.
c. Inform risk assessment models about how corresponding changes in fire cue perception from different fire growth rates affect perceived risks.

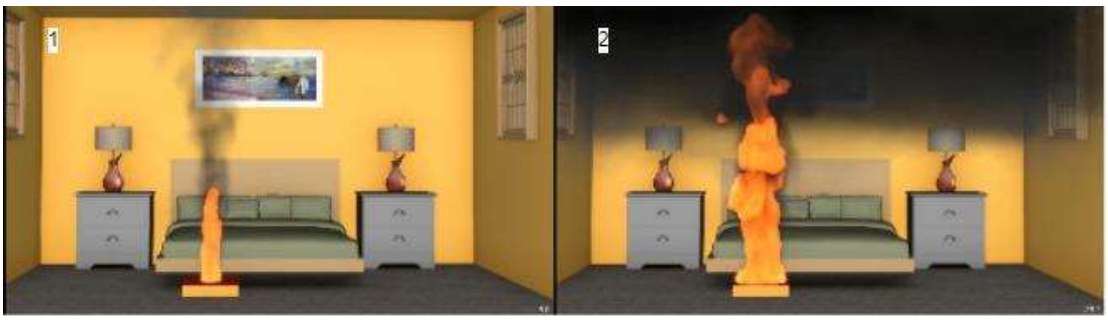

Figure 1: Comparison of visuals at different stages in a growing fire. Top: Shot at 13 seconds in a fire growing at a 'Warp' rate. Bottom: Shot at 29 seconds; a fire growing at a 'Warp' rate.

1.1 Objective

The principal objective of this study is to produce realistic movies of fire and smoke in different surroundings, which will be used to perform human behaviour experiments. FDS is a very useful tool when the objective is to obtain quantitative data from a simulation, as is the case with most projects dealing with the built environment[11]. Seemingly, this could be why professional engineers and research scholars so widely use it. However, when it comes to working with 3D objects in a simulation, the visuals are not very realistic. This is primarily because Smokeview (a free tool developed by NIST to view FDS results) displays objects in the form of cube/cuboid grid cells, and doesn't have the capability to display smooth textures or contours.

Psychological experiments at MSU will include participants watching video animations created from the library of simulations and answering a set of carefully

structured questionnaires. The answers will be used to understand how accurately humans understand the visual cues of fire in terms of growth rate and severity.

1.3 Pyrosim

. PyroSim is a graphical user interface (GUI) for the Fire Dynamics Simulator (FDS) software developed by Thunderhead Engineering. PyroSim provides a user-friendly interface for building and editing FDS models, setting up simulations, and visualizing the results[12]. It has the capability to easily import 3D files (DWG, DXF, 3DS,STL,OBJ,SKP and DAE) into the computation domain and generate a FDS input file that includes the imported objects.

For this study, Pyrosim was used to build the model and generate FDS input files. The simulations were run on the University of Maryland's High-performance Computing (HPC) cluster called Zaratan. The results of the simulation were downloaded and processed in Pyrosim Result Viewer.

Chapter 2: The Model

2.1 Simulations

A set of simulations was performed in this study to establish a library. Movies will be created using this simulation library to conduct experiments on human behavior at Morgan State University. This represents an example of a non-immersive virtual reality application. These simulations will be conducted to model the growth rate of fire in its early phase until it reaches 1 MW. Four distinct rooms have been designed to simulate fires in this study: a bedroom, a living room, a kitchen, and an office. Each of the four rooms will be simulated at six different growth rates of fire: slow, medium, quick, fast, ultra-fast, and warp. This will result in a total of 24 fire simulations for this study.

2.2 Material of Reaction

Polyurethane (GM27) has been considered as the material for reaction since it is very common to have polyurethane in upholstered furniture in surroundings considered for this study. The yields of the products of combustion (see Table 1) have been borrowed from Table A.38 and A.39 of the SFPE Handbook of Fire Protection Engineering (2016 edition)[2].

Table 1: Combustion properties of GM27 Polyurethane, borrowed from Table A.38 and A.39 of the SFPE Handbook of Fire Protection Engineering (2016 edition).

Property	Value
C	1
H	1.7
O	0.3
N	0.08
Soot yield	0.192
CO yield	0.042

2.3 Heat Release Rate

The most widely used parameter to define the intensity and behaviour of a fire is the Heat Release Rate (HRR). It is considered the single most important variable in characterising the 'flammability' of products and their consequent fire hazard[13].

Typical design fire curves often use 't-squared' approximations to describe the heat release rate of accidental open flaming fires. In a 't-squared' growth, the heat release rate varies proportionately to the square of time. Further, the 't-squared' growths are classified as slow, medium, fast, and ultra-fast based on the time required to grow to a heat release of 1000 Btu/sec (1055 kW)[14]. See Table 2

$$q = \alpha t^2 \quad (1)$$

where;

q is the heat release rate (in Btu/sec or kW)

α is the constant governing the speed of growth

Table 2: Times required of different types of growths and the corresponding 'α's.

Class	Time (sec) to reach 1000 Btu/s	α
Slow	600	0.0029
Medium	300	0.0117
Quick	204	0.025
Fast	150	0.047
Ultra-fast	75	0.19
Warp	40	0.66

The category 'Quick' and 'Warp' have been added for this study to expand the variability of results. Figure 2 shows the plot of HRRs for the mentioned classes of growth rates.

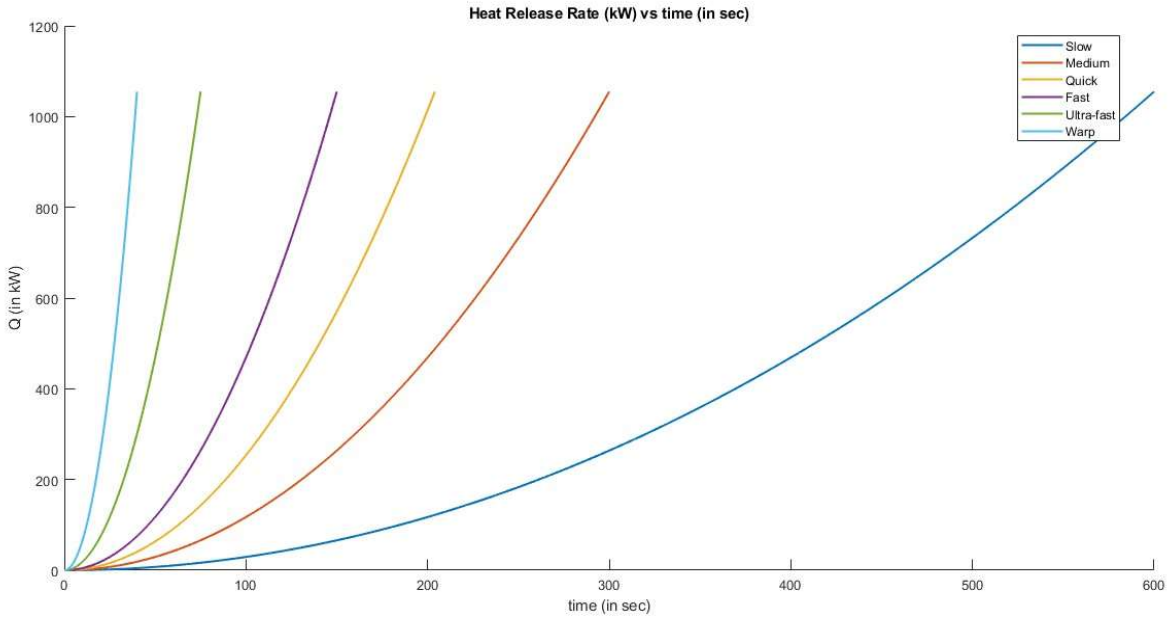

Figure 2: Heat Release rate vs time for different categories of growth rates.

2.4 RAMP & SPREAD_RATE

One method to simulate a 't-squared' heat release rate in FDS is by using the RAMP function. An elementary example of using the RAMP function to create an ultra-fast growth heat release rate can be found in Appendix A. In the example in Appendix A, a fire obstruction is set up in a computation domain of size 5 meters by 5 meters by 3 meters (high). The chemical reaction parameter in the input file is for polyurethane, and is borrowed from the SFPE handbook[2]. The Heat Release Rate (HRR) RAMP is set up in accordance with the 'ultra-fast' growth such that the heat release rate reaches 1055 kW in 75 seconds. The output HRR from the simulation has been plotted in Figure 3.

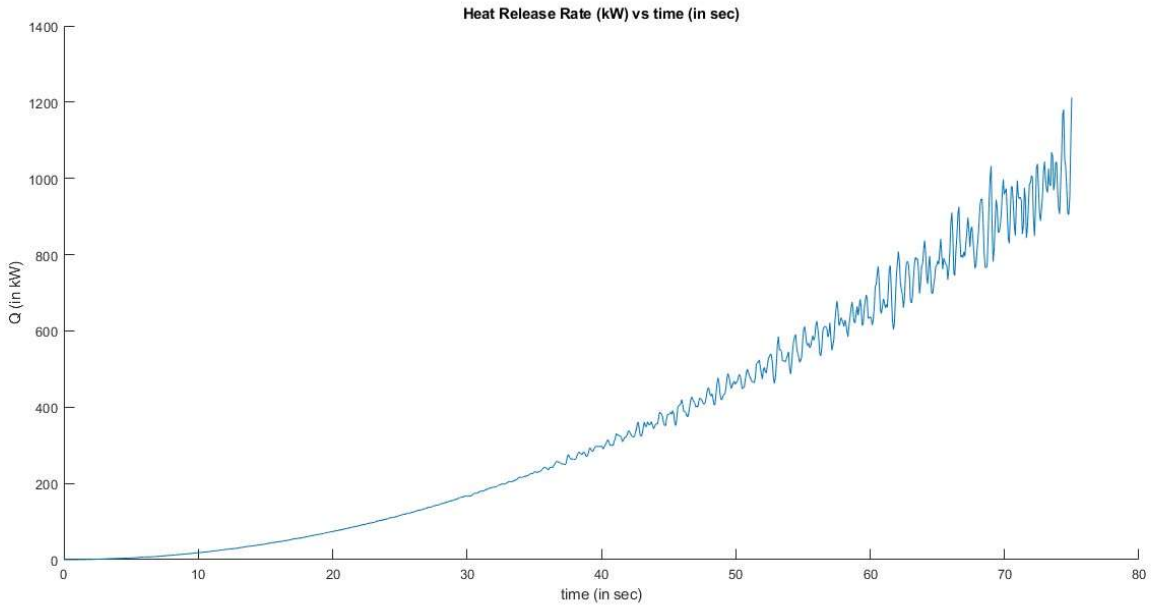

Figure 3: Heat Release rate vs time for simulated example (see Appendix A) for an ultra-fast growth rate fire.

A radially spreading fire can be simulated in FDS using the SPREAD_RATE function. This function can be added to the VENT line along with the origin of the fire and the rate of radial spread in units of meter/second. The idea of using the SPREAD_RATE function is to mimic the radially spread fire more naturally. The visuals created using SPREAD_RATE in a simulation look similar to a real-life spreading fire.

Although FDS User Guide does not recommend using the SPREAD_RATE to mimic a 't-square' growth, the SPREAD_RATE can be carefully manipulated to do it. This manipulation is based on research work that establishes the relationship between SPREAD_RATE and the parameter 'α' described previously[15].

Since the requirement of this study is to create life-like movies, a relationship between SPREAD_RATE and α was used to make a radially growing fire follow a 't-squared' growth curve. Here is the derivation of the relationship between SPREAD_RATE and α by Ciani and Capobelli (2018)[15]:

$$SPREAD_RATE = \frac{dr}{dt} \tag{2}$$

Where:

r is the radial distance from the center of the fire

t is time in seconds

Using (1) , (2) can be written as s

$$SPREAD_RATE = \frac{dr}{dt} \times \frac{\pi r^2}{\alpha t^2} \times \frac{HRRPUA}{1}$$

Or, $SPREAD_RATE \times \int_0^t t^2 dt = \frac{\pi}{\alpha} \times \frac{HRRPUA}{1} \times \int_0^r r^2 dr$

Or, $SPREAD_RATE \times \frac{t^3}{3} = \frac{\pi}{\alpha} \times \frac{HRRPUA}{1} \times \frac{r^3}{3}$

Since, $SPREAD_RATE = \frac{r-0}{t-0}$

Or, $SPREAD_RATE^2 = \frac{\alpha}{\pi} \times \frac{1}{HRRPUA}$

Therefore, $SPREAD_RATE = \sqrt{\frac{\alpha}{\pi} \times \frac{1}{HRRPUA}}$ (4)

Using (4) for an ultra-fast 't-squared' fire growth:

α = 0.1875556

And

$$SPREAD_RATE = \sqrt{\frac{\alpha}{\pi} \times \frac{1}{HRRPUA}} == \sqrt{\frac{0.1875556}{\pi} \times \frac{1}{1055kW}} = 0.007522527781$$

The previous example (Appendix A) was modified by replacing the RAMP with SPREAD_RATE = 0.007522527781 (see Appendix B). Figure 4 compares HRR outputs from simulations using RAMP and SPREAD_RATE function.

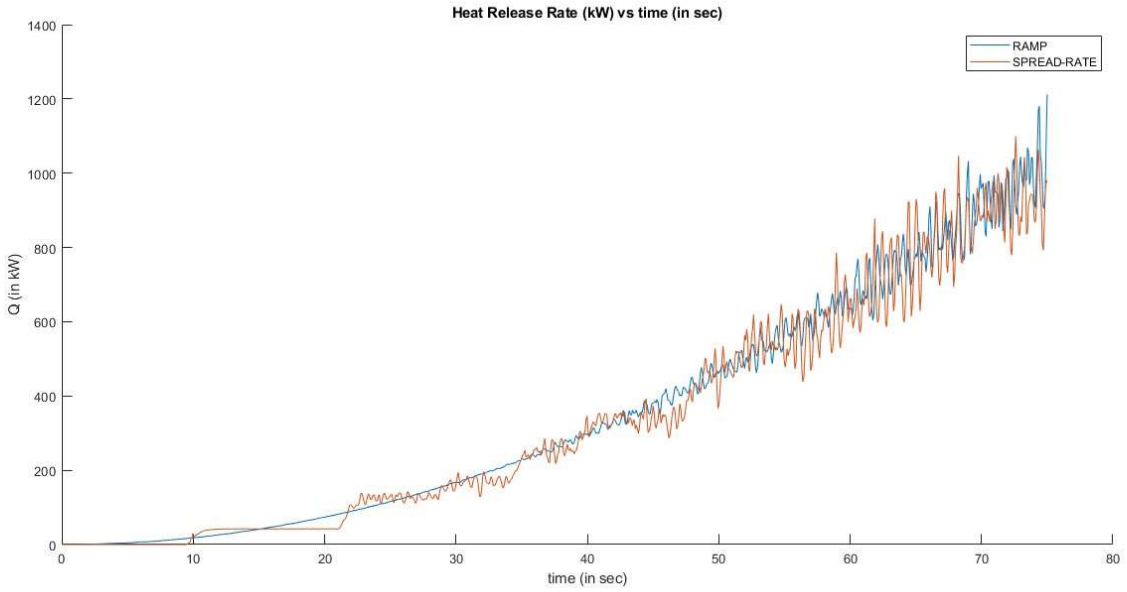

Figure 4: Heat Release rate vs time for simulated example using RAMP and SPREAD_RATE

It can be observed that even though the SPREAD_RATE function was used, the HRR curve nearly overlaps the output HRR curve from the RAMP function. It is worth noting that there are certain time steps at which the two curves do not coincide. Still, the benefit of generating more realistic visuals, which is very important to this study, supersedes the anomaly.

2.5 Simulation Time

Each growth rate case was simulated until the fire reached 1000 Btu/s or 1055 MW. See Table 2.

2.6 The Computational Domain

The empty room is 5 meters wide, 5 meters long and 2.8 meters high. Different three-dimensional objects are placed in the room to make it look like a different type. It should be noted that the wall dimensions and the relative position of the fire obstruction have been maintained to be the same for different types of rooms.

The following are the different types of rooms considered for this study:

1. Bedroom
2. Living Room
3. Kitchen
4. Office

Figure 5 shows different room types. The 3D files used in this study were downloaded from *Turbosquid.com*[16] in *.obj* format.

2.5 Fuel Source

The size of the fuel source for this study is 0.5 meters by 0.5 meters. A few tests were done with bigger obstructions. But, keeping in mind the dimensions of the room, the mentioned size appeared to be more appropriate.

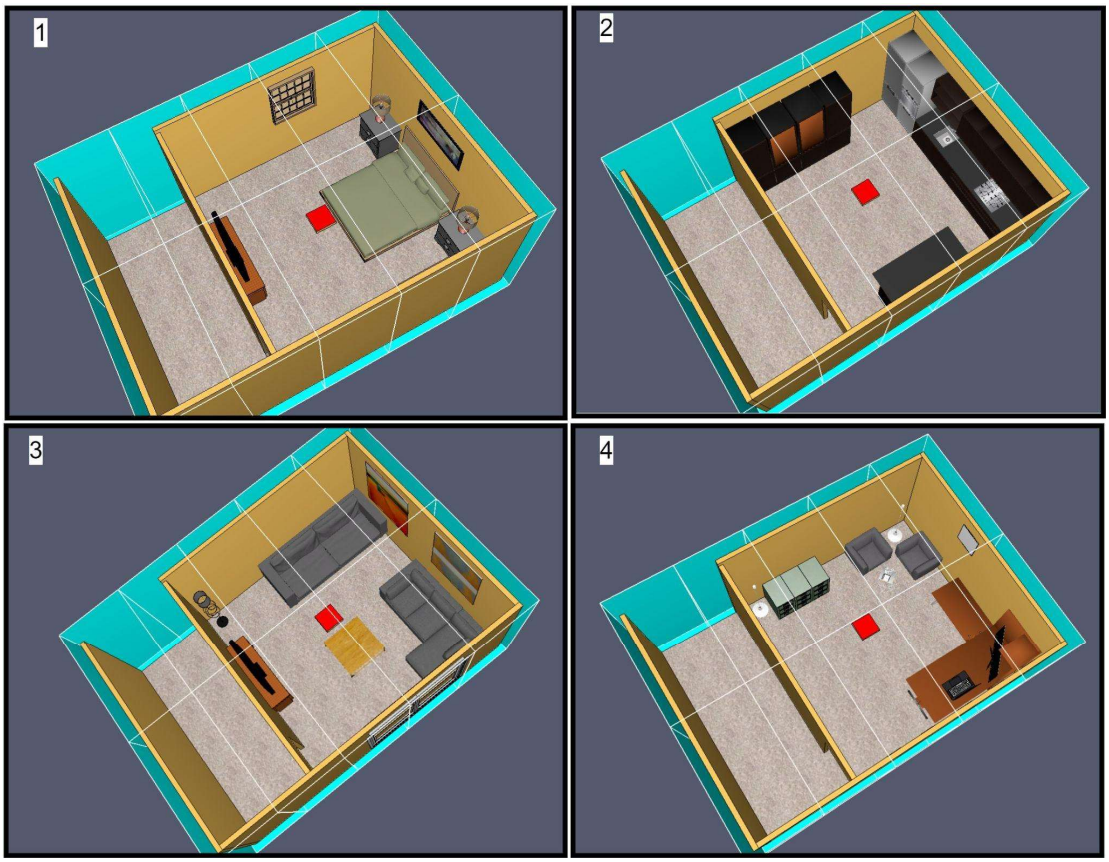

Figure 5: Different types of room configurations. Top left: Bedroom, Top Right: Kitchen, Bottom Left: Living Room, Bottom Right: Office.

Chapter 3: Data Collection

3.1 Point of View

A total of seven positions were chosen at which an observer can be positioned and look at the fire obstruction. The positions are at 1-meter intervals from the fire obstructions along two imaginary lines, one running from the fire location towards the entrance and one line to the other corner. See Figure 6.

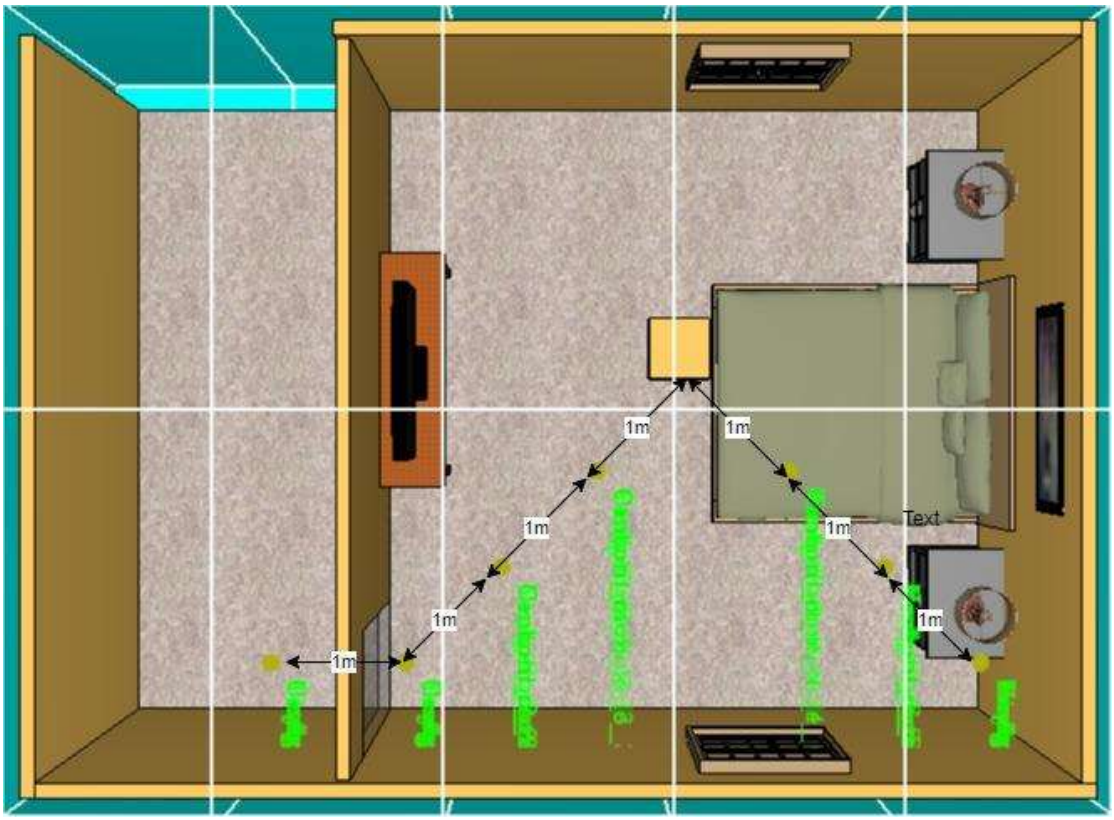

Figure 6: Location of observers (yellow dots), the green text represents the description of the device.

The height of the point of view is set as 162.29 cm based on average height data by CDC[17]. See Table 3 and Figure 7.

Table 3: Calculation for an average height of eye base on CDC data.

	Height (cm)	Forehead (cm)	Eye (cm)
Average male	175.26	6.14	169.12
Average female	161.29	5.83	155.46
Average height of eye			162.29

Figure 7: Height of observer.

The DEVC function in FDS has been used to capture data by placing devices at the observer's point of view.

Pyrosim's 'Roam' tool allows the observer to move into the model like real people. A typical view of the fire obstruction from the point of observation (using Roam tool) is shown in Figure 6.

Figure 8: A typical view of fire obstruction from the point of view near the door.

Another method of placing the observer at a desired position is by modifying the *.view* file from the simulation output folder. The detailed process for modifying the *.view* file can be found in Appendix C (credits: Dr. Justin Bonny, Morgan State University).

3.2 DEVC & SLCF

The following data is collected from devices placed at the point of view of the observer:

a. Temperature
b. Heat Flux
c. Oxygen
d. Carbon Monoxide
e. Carbon dioxide
f. Visibility

The data was collected at every frame of the simulation. Figure 9 shows the plot of visibility vs time for a warp growth rate fire in a bedroom set-up.

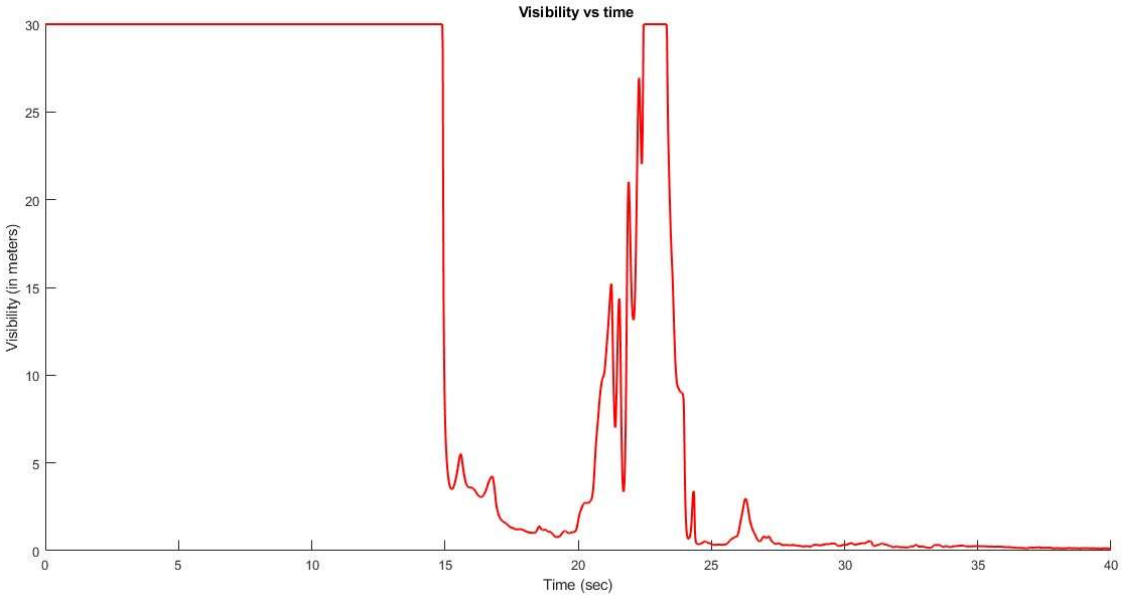

Figure 9: Visibility vs time for warp growth rate in bedroom setup.

Slice files are a great way to collect and visualise data. The above-mentioned data have been collected in the slice files for all the simulations. The slice files are in *.sf* format and can be parsed using the *slread.m* function to obtain the data in three-dimensional arrays[18]. See Appendix D for a sample script using the *slread.m* function.

Chapter 4: Resolution

4.1 Mesh size

The first test case was run with 5 cm grid cells. This setup resulted in a total of 1.15 million cells. Although a 5 cm cell size has a great saving in terms of computation time, coarse grid cells resulted in a lesser realistic simulation when compared to a 2.5 cm grid resolution.

The 2.5 cm gird cell size results in a total of 9.24 million cells and rendered a more realistic visual of the flame and smoke. Figure 11 compares 2.5 cm grid cells and 5 cm grid cells for ultra-fast growth rate in bedroom setup.

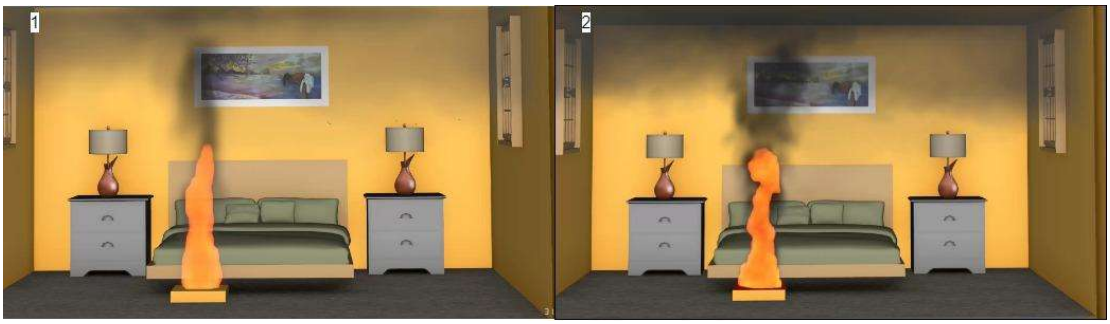

Figure 10: Comparison between 5 cm and 2.5 cm grid cells. Left: 5 cm grid cells, Right: 2.5 cm grid cells.

Considering the importance of the quality of visuals for this study, the 2.5 cm grid size was selected for the simulations. The 9.24 million cells have been divided into 10 different meshes, with each mesh being assigned to a different thread using the mpi process on Zaratan[19].

4.2 Computation Time

A total of 1369 seconds of simulation time is required for one configuration (See Table 2). Therefore, a total of 5476 seconds (4 x 1369 seconds) of simulation time is required for all four room settings. Based on a test case of a 75-second simulation with 60 frames per second, Table 4 shows the estimated CPU times.

Table 4: CPU times

Simulation Time	CPU Time (sec)	CPU Time (hours)
75 sec	1,421,000	394.72
5476	103,619,320	28,783.14

4.3 Frames per second

A standard video has 24 frames per second. Initially, two test runs were done with 30 and 60 frames per second for this study. The 60 frames per second setting was selected because it has a more life-like feel. Snapshots may not be the best way to judge, and one must see the videos to understand the difference.

Figure 11 shows the fire in action in all four room configurations from the point of view of an observer.

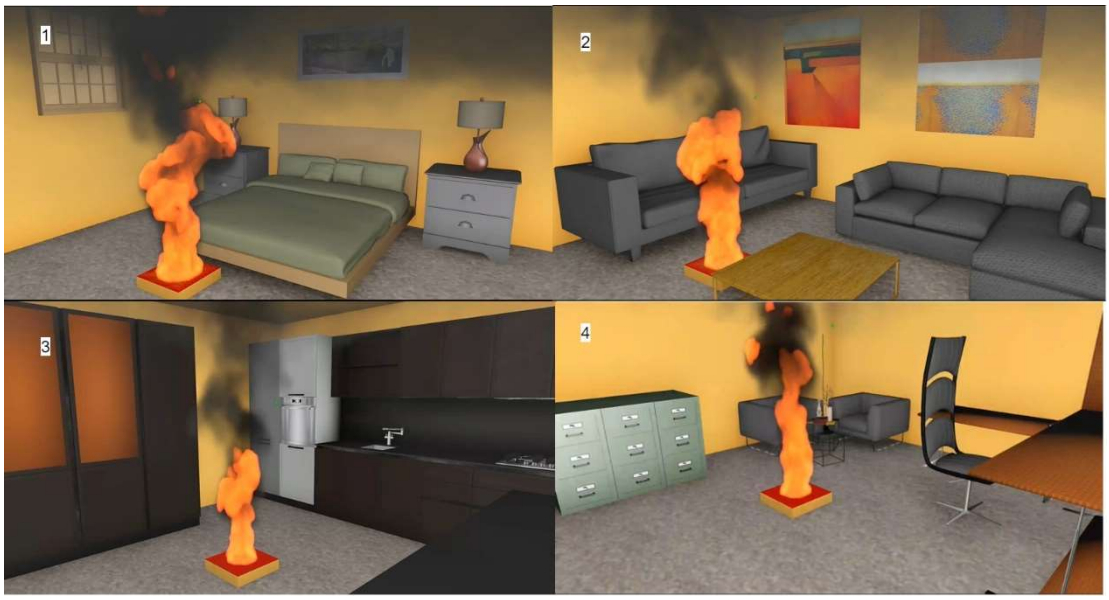

Figure 11: Fire from the point of view of an observer; Top left: Bedroom, Top Right: Living Room, Bottom Left: Kitchen, Bottom Right: Office.

4.4 Fire Simulation for Response Assesment

The simulation outcomes are being utilized to create movies that will be employed in experiments at Morgan State University. These movies will serve as visual aids that can help observers comprehend the behavior of fires more effectively. Furthermore, the experiments will evaluate the decision-making abilities of the observers in the context of a fire emergency.

During the experiments, the observer will be situated at specific locations that are marked by yellow dots in Figure 6. From these locations, the observer will be able to observe the flame and smoke and provide answers to a set of carefully structured questions. These questions have been designed to assess two primary categories: the severity and intensity of the fire and the observer's intended course of action.

The first category seeks to evaluate the severity and intensity of the fire by taking into account any associated risks or dangers that may arise. By analyzing the fire's characteristics, the observer will be able to assess the potential danger posed by the fire and determine whether any safety measures need to be taken.

The second category pertains to evaluating the observer's planned course of action based on the information obtained from the fire's characteristics. By responding to the questionnaire, the observer's decision-making process will be assessed, including their ability to identify the appropriate safety measures and respond to the emergency effectively.

By analyzing both the fire's characteristics and the observer's questionnaire responses, valuable insights can be obtained regarding their ability to accurately perceive the visual cues of a developing fire.

Chapter 5: Conclusion – NSF Project

The main goal of the study conducted by the team on the UMD side was to produce highly realistic simulations, which required multiple trials to achieve. Creating visual simulations is a subjective process that is heavily influenced by the specific requirements of the project. This aspect of FDS had not been extensively explored before, so the experimentation process allowed the team to gain a better understanding of the challenges involved and identify the most effective methods for creating life-like simulations.

When using 3D objects for fire simulations, it is important to consider the format in which they are available. Among various formats, the .obj format has been found to work better than others. It is also recommended to select objects with fewer sub-components to make handling them in Pyrosim easier. The surface texture of the objects is another crucial factor that influences their realism, and it is suggested to conduct trials with different surface textures before running the final simulations. While free 3D object files are available online, they are limited in number, and purchasing files may provide more options to choose from.

Certain 3D objects contain enclosed spaces that can result in pressure zones within simulations, leading to numerical instability. Therefore, it is important to be cautious when selecting 3D objects, and ideally, those with enclosed spaces should be avoided altogether. However, this may not always be feasible, and in such cases, creating small holes in the objects can help to resolve the issue.

Chapter 6: Introduction- The Lagrangian Model Project

6.1 Background

FDS provides users with various options to create a fire suppression system based on the requirements of their project. For this study, the chosen model involves suppressing fires by determining the amount of water needed to impinge upon the fire's surface. Additionally, the amount of water carried by each particle (represented by a numerical droplet) is determined by the rate at which particles are injected through a nozzle or sprinkler.

A critical parameter to characterize sprinklers and nozzles in FDS is PARTICLES_PER_SECOND. It determines the number of droplets inserted per active sprinkler or nozzle and has a default value of 5000 pcs/s. FDS monitors introduced numerical droplets (Lagrangian particles) which represent many more actual droplets.

The number of physical droplets represented by a numerical droplet can be calculated by: $F = \frac{\dot{m}_{water}}{m_{actuak\ droplet}} \times \frac{1}{PPS}$

$$F = \frac{\dot{m}_{water}}{m_{actuak\ droplet}} \times \frac{1}{PPS}$$

Where:

F is the number of actual droplet represented by one numerical droplet

$\dot{m}_{water}$ is the mass flow rate of water coming out of the nozzle or sprinkler

$m_{actuak\ droplet}$ is the mass of an actual physical droplet

PPS is the particle injection rate defined by PARTICLES_PER_SECOND

For the default setting of PARTICLES_PER_SECOND and the sprinkler characteristics defined in 7.1, each numerical droplet would typical carry 3600 actual droplets.

In some cases, the value of PARTICLES_PER_SECOND may be low, making the effect of droplets within a grid cell more intermittent, thereby changing the gas temperature rapidly in a single time step bringing disturbances in simulated temperatures or resulting in numerical instability.

The central idea of this study is to find whether the default value of PARTICLE_PER_SECOND is good enough for all grid sizes and to find how grid size and PARTICLE_PER_SECOND work together to impact the accuracy of results.

6.2 Hypothesis

For a fixed particle injection rate, if the grid cell's size is decreased, fewer particles will pass through a grid because of the reduced grid size. Consequently, there could be some time steps at which no particles would cross the grid cell.

The presence of variability in the mass flux passing through a computational cell can be explained by the occurrence of such time steps, in which no particles pass through the cell. This is because the size of the computational cell is too small to capture the entire range of particle motion, resulting in fluctuations in the computed mass flux.

Since the mass flux calculation involves averaging the mass of particles passing through the cell over a certain period of time, the absence of particles during some time steps can result in significant variations in the computed mass flux. Therefore, it is hypothesized that increasing the rate of particle injection could reduce the noise in reading the characteristics, thereby improving the accuracy and reliability of simulations or calculations that rely on mass flux data.

Chapter 7: The Computation Domain

7.1 The Setting

The setup for this study is a modified version of the 'bucket_test', from the library of examples provided by FDS[20]. The computation domain is 10 meters long, 10 meters wide and 6 meters high. An upright sprinkler is mounted at the centre of the ceiling, at 0.1 meters below the ceiling. The spray pattern has been specified as 'Uniform' for simplicity. Also, the spray angle is 0 to 90. The nozzle flow rate is 180 litres per minute or 3 kg/s. The diameter of the droplet was chosen to be 1000 μm for the study.

This setup has three iterations in total – without any fire, with a fire located below the nozzle, and the last one with the fire located at an offset distance of 1.5 meters from the center-line of the nozzle. Figure 12 shows the three configurations.

7.2 Grid Sizes

Since the central idea of this study is to understand how the variation of particle injection rate and grid size impacts accuracy; three different grid sizes were used for the analysis; 0.1 m, 0.2 m and 0.4 m. Figure 13 gives a representation of the mesh resolution compared to the computation domain.

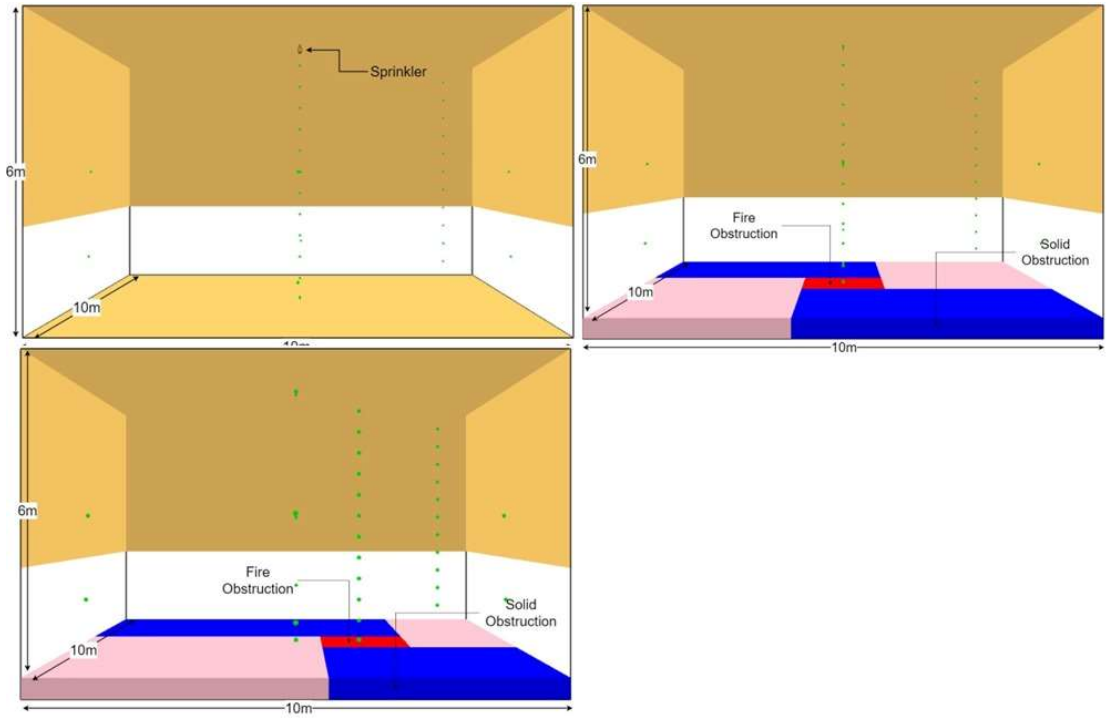

Figure 12: Top Left: Setup with no fire. Top Right: Setup with fire below the nozzle. Bottom Left: Setup with fire offset from the center of the nozzle

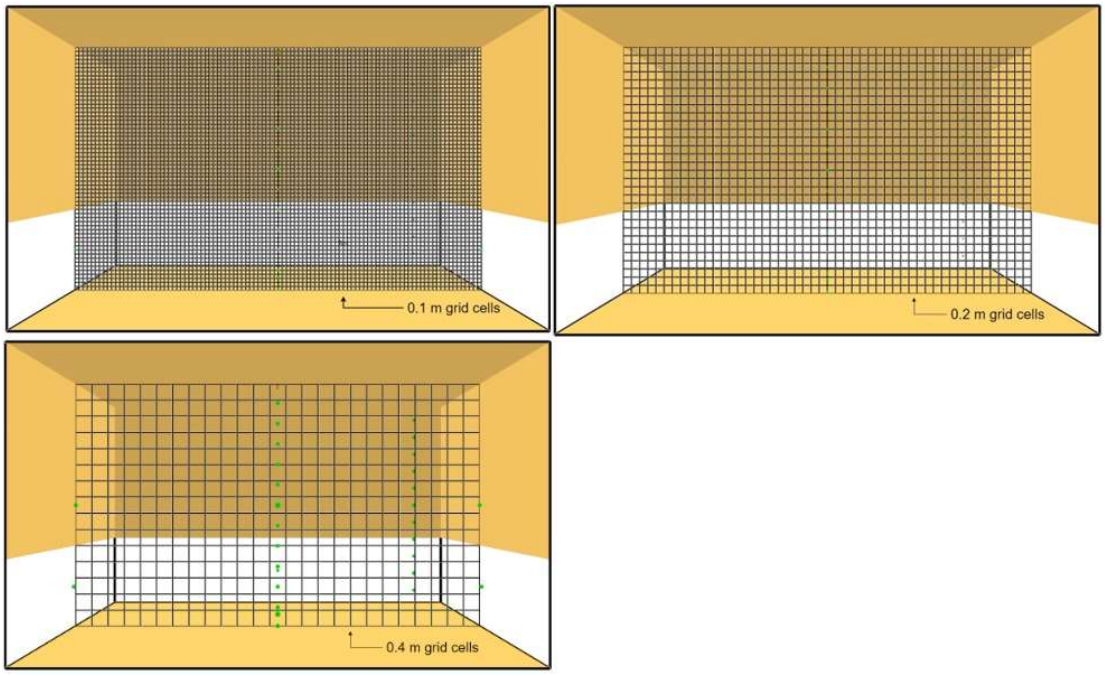

Figure 13: Top Left: 0.1m cells. Top Right: 0.2m cells. Bottom Left: 0.4m cells

7.3 Paticle Injection Characteristics and Rate

The water spray system in question ejects water at a rate of 180 liters per minute. By default, the size distribution of the water droplets is set to 'ROSIN-RAMMLER-LOGNORMAL', which is a combination of the 'ROSIN-RAMMLER' and 'LOGNORMAL' distributions. In the input file, the median size of the droplets has been defined as 1000 micrometers on the PART line. However, instead of specifying the size of the nozzle, the initial drop velocity has been defined using the PARTICLE_VELOCITY parameter, which has been set to 10 m/s.

To simplify th e spray pattern, the SPRAY_ANGLE parameter has been set to range from 0 to 90 degrees, ensuring that the droplets are ejected within a hemispherical region. Additionally, the SPRAY_PATTERN_SHAPE parameter has been set to 'UNIFORM', which results in the droplets being ejected evenly throughout the hemispherical region. By combining these parameters, a uniform and efficient spray pattern is achieved, with droplets of the specified median size being ejected at a constant velocity.

The simulations without fire were tested for 10, 100, 400, 700, 1000, 2000, 3000, 4000, 5000, 6000, 7000, 8000, 9000, 10000, 15000, 20000, 25000, and 30000 particles per second for all three grid sizes mentioned previously. Figures 14 to 16 show how Lagrangian particles look in different configurations.

The simulations with fire were tested for 3000, 9000 and 30000 particles per second for the three grid sizes. The reason for testing for just three particles per second variation is discussed later.

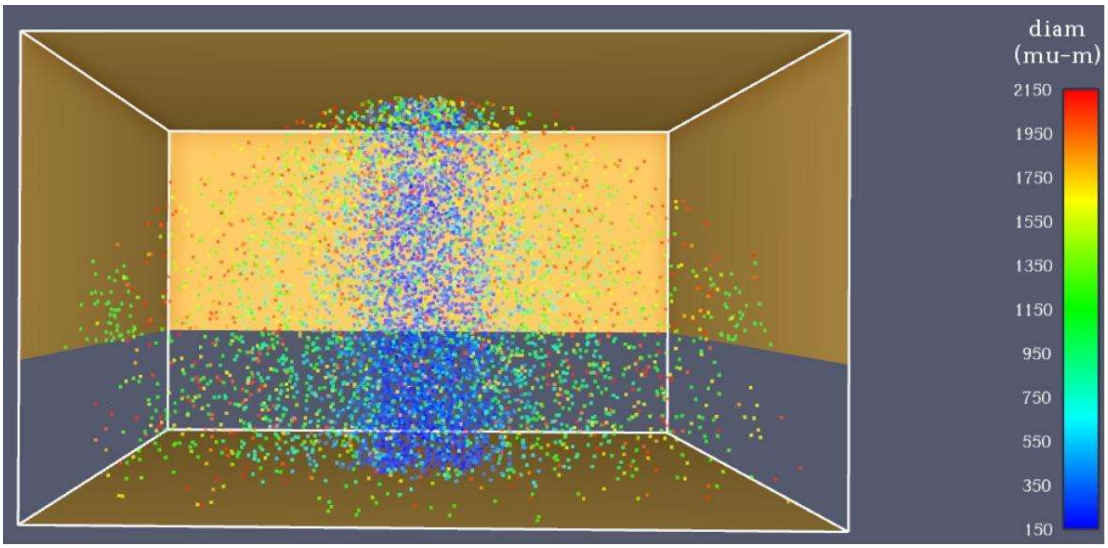

Figure 14: 5000 Particles/s without a fire.

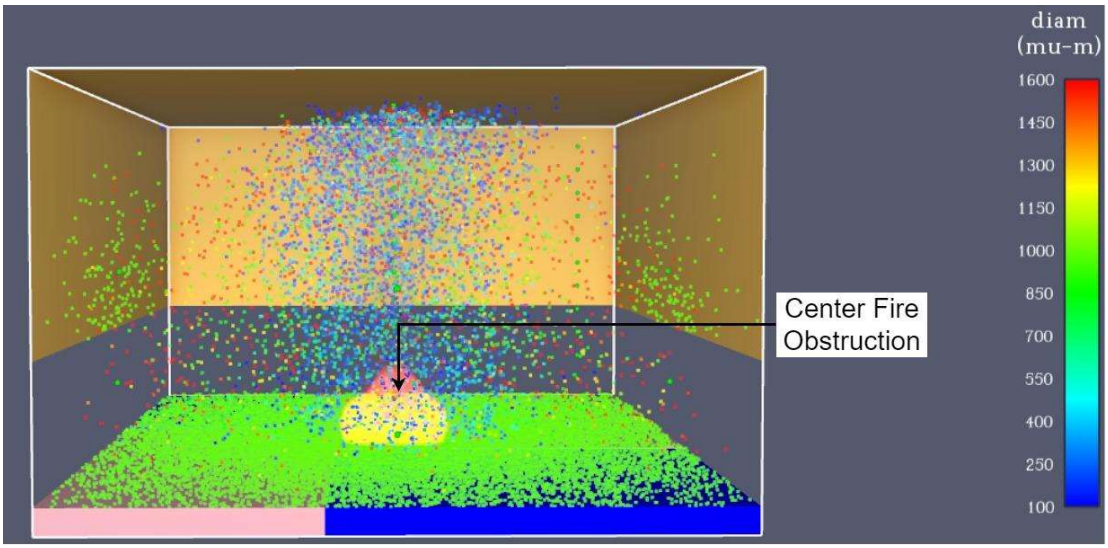

Figure 15: 5000 Particles/s with a fire below the nozzle.

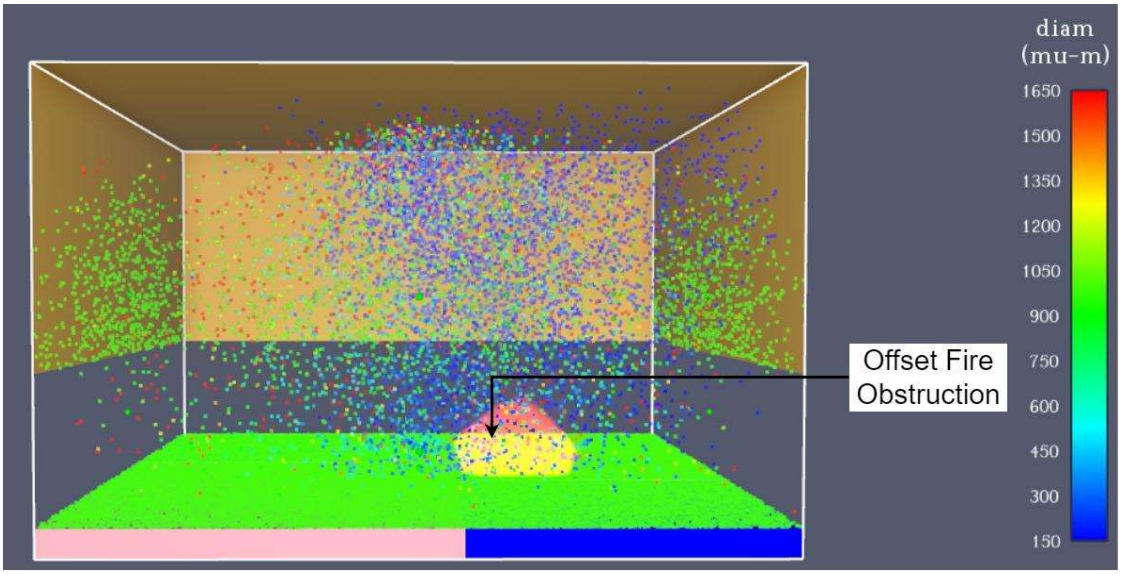

Figure 16: 5000 Particles/s with a fire offset from the center of the nozzle.

7.4 Simulation Time

The simulation time for all the simulations is 120 seconds. The number of frames, controlled by NFRAMES, is set at 12000, which provides 12000 data points through devices and slice files.

7.5 Location of Slice

A slice file is placed at 0.1 meters above the floor level and uses the 'PARTICLE FLUX Z' diagnostic in FDS, which measures the mass flux of particles passing through the slice in units of kg/m^2-s.

For 0.1 meters grid size, the slice file renders a three-dimensional array of dimensions 101 x 101 x 12001. Similarly, for 0.2 and 0.4 meters grid sizes, it provides an array of 51 x 51 x 12001 and 26 x 26 x 12001, respectively.

Chapter 8: Analysis

8.1 Mass Conservation

The first step of the analysis was to check whether the mass flow rate of water coming out of the nozzle is equal to as specified for the simulation (3 kg/s). Two kinds of devices were used to check mass conservation.

Accumulated Mass Per Unit Area (AMPUA) captures the mass accumulated in a specified area over a period of time. FDS also allows calculating the AMPUA over an area by using SPATIAL_STATISTIC = 'SURFACE INTEGRAL'. AMPUA has units of kg/m^2, and when integrated over an area using 'SURFACE INTEGRAL', it renders the data in units of kg.

The other diagnostic used is 'PARTICLE FLUX Z'. It records the integrated mass flux of all the particles passing through the given plane. It has units of kg/m^2-s; when integrated into an area using 'SURFACE INTEGRAL', it provides the result in units of kg/s.

These devices were placed on all six facades of the computation domain (see figure 17). The sum of the data from all the sides was plotted against time to check whether the mass was correctly conserved. Figures 18 and 19 show a typical plot to check mass conservation, using PARTICLE FLUX Z and AMPUA respectively. It can be noted that the average stays at 3 kg/s which was specified for the simulation.

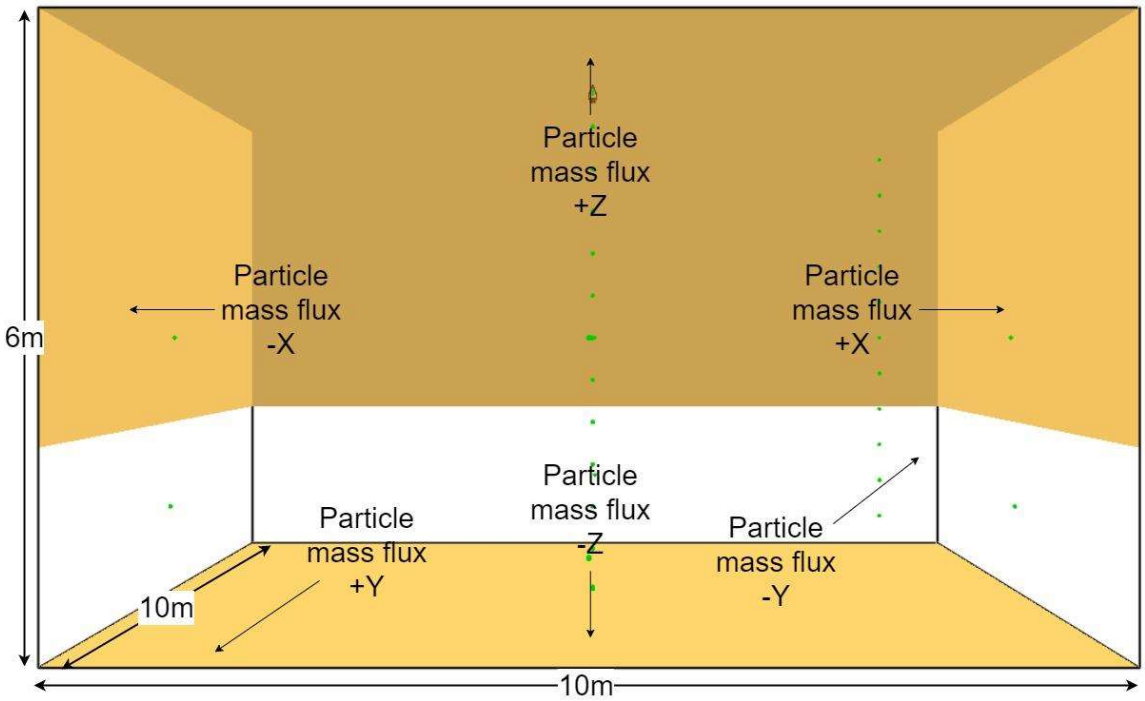

Figure 17: Location of devices in the computational domain to check the conservation of mass.

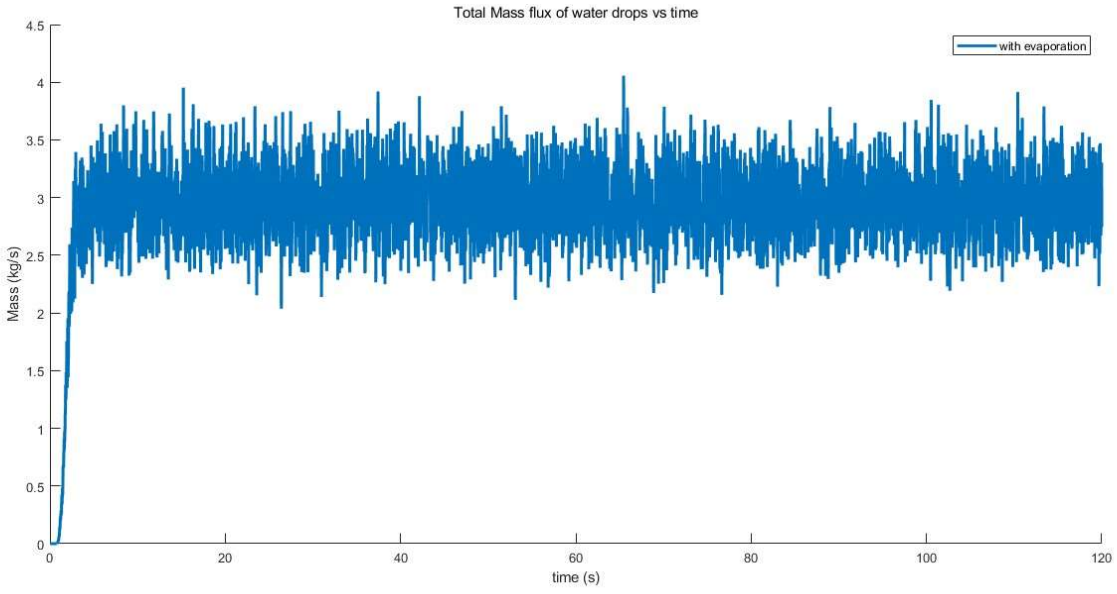

Figure 18: Mass conservation using 'PARTICLE FLUZ Z'

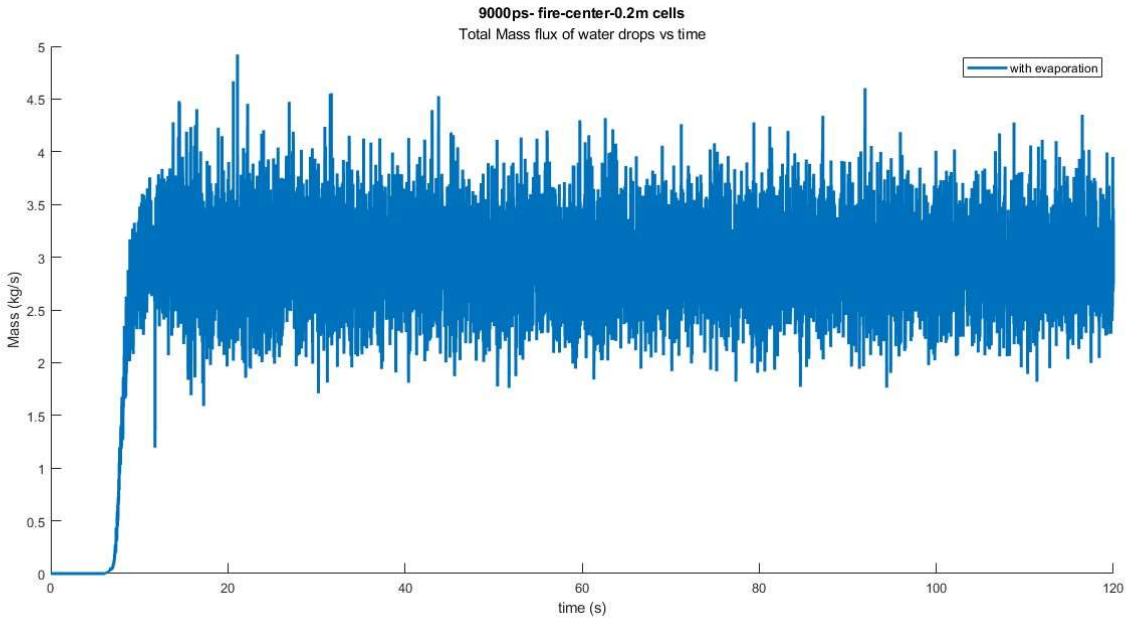

Figure 19: Mass conservation using 'AMPUA'

It is worth noting that when using 'SURFACE INTEGRAL' to capture data with AMPUA, the units of measurement are in kilograms (Kg). In Figure 19, the plot represents the rate of change of the captured data over time, specifically the derivative of the data points.

8.2 Reading the Slice Files

Slice files are a great way to visualize the results of simulations in FDS. A typical view of a slice file is shown in Figure 20. FDS also allows extracting data from slice files using the 'fds2ascii' program[11]. However, the program was not used to read the slice files in this project. A Matlab-based function called 'slread.m'[18] was used to read the slice file because of the ease of post-processing of data (see Appendix D). The inputs to 'slread.m' are the .sf file, start and end times. One of the outputs from this script is a three-dimensional array. The x and y direction of the array represents the grid cells,

and the z dimension represents the variation in time. The other output is the array of time steps.

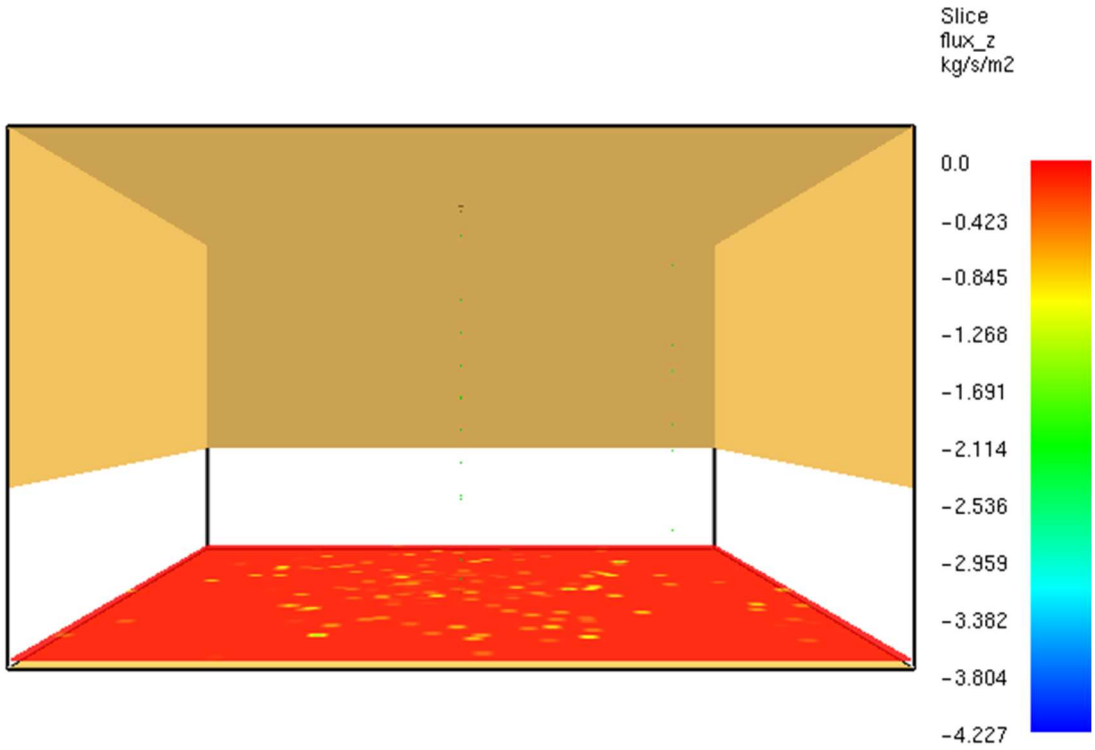

Figure 20: A slice file at Z=0.1m showing the water mass flux in the Z direction

8.3 Mean Mass Flux

The slice file at Z = 0.1 m contains 12001 data points (every 0.01 second) of mass flux for every cell. The time-averaged mean of mass flux at every cell gives the idea of the spatial distribution of particles (i.e., the mass accumulation of particles falling across the floor area). See Figure 21.

The projection of the mean of mass flux provides a very good quantitative and qualitative picture of the distribution of water particles across the floor area. A drawback of this plot is that it does not provide an easy way to compare the data across different settings of particle injection rates and grid sizes.

For comparing data across different settings of particle injection rate and grid sizes, a line cell that passes through the centre of the floor has been considered, as shown in Figure 22. It's worth noting that the chosen line of cells intersects with the slice file, and it traverses through the center of the room in a way that keeps it positioned above the fire obstruction. This line's trajectory, which remains above the fire obstruction, indicates that it passes through the area immediately above the flames' source, as well as the center of the room. This information is particularly relevant for simulations involving fire, as it provides insight into the location of the line with respect to the fire and the room's layout.

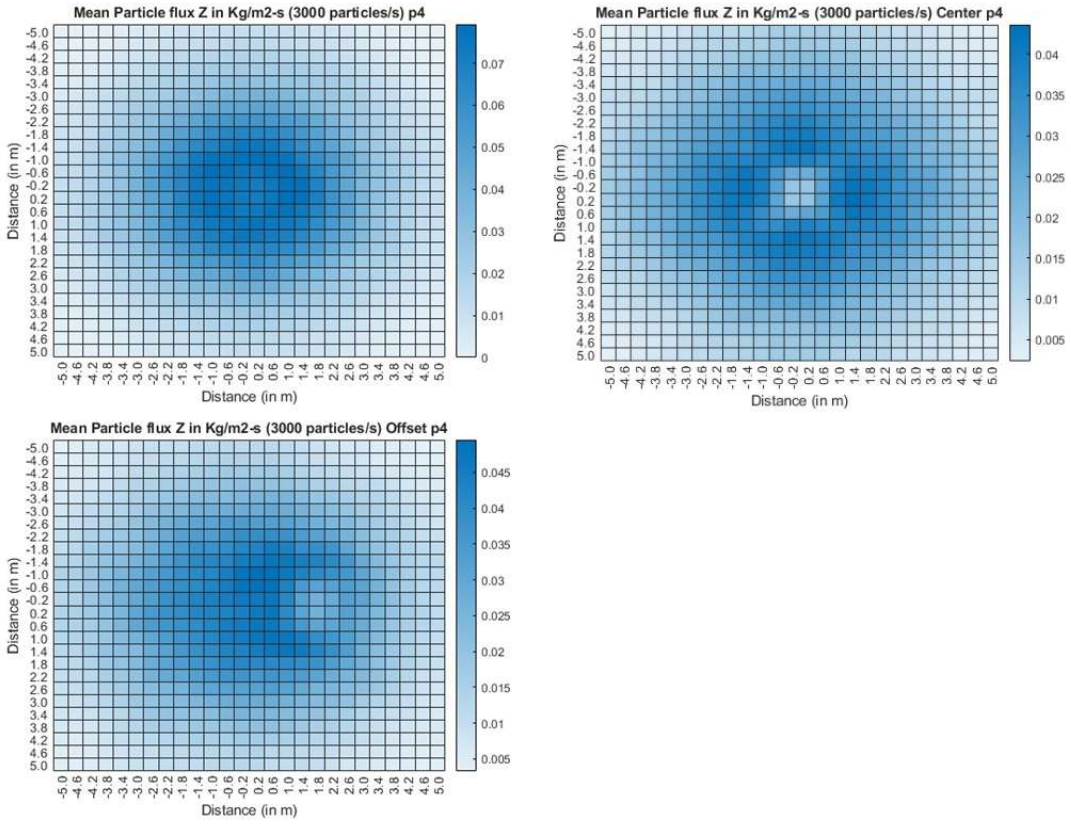

Figure 21: A slice showing the mean particle mass particle mass flux at Z = 0.1

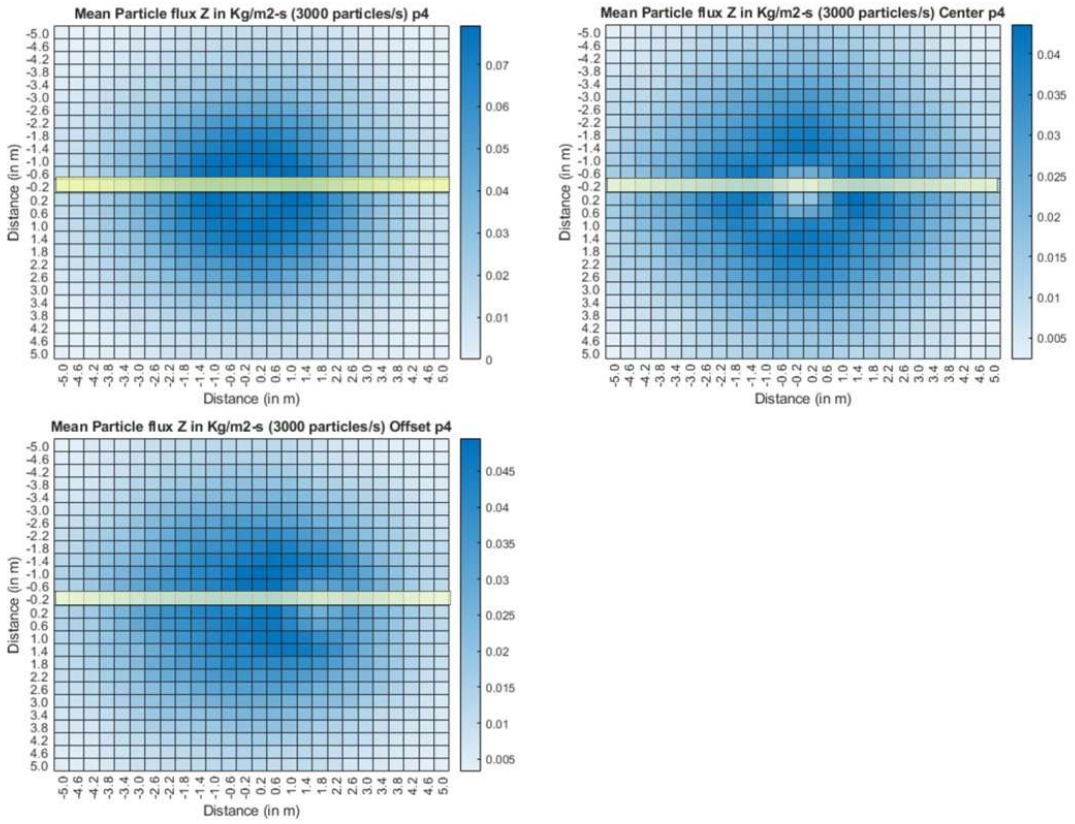

Figure 22: A slice showing the mean particle mass flux at Z=0.1 meters with the line of cells considered for analysis shown in yellow.

8.4 Variability in Mass Flux

Variability (also called diversity, uncertainty, dispersion, and spread) is the extent to which data values differ from one another. It indicates how close to this central size measure the data values typically are. If all data values are identical, then the variability is zero. The more spread out things are, the larger the variability[21].

The Population (or Sample) Standard Deviation is the traditional choice for measuring variability, summarizing the typical distance from the average to the data values. It indicates the extent of the randomness of individuals about their common average[21].

The sample standard deviation is defined by the equation:

$$\sigma = \sqrt{\frac{\Sigma(X_i - \mu)^2}{N}}$$

Where:

σ is the sample standard deviation

X_i is the data point

μ is the mean

N is the total number of data points

The plots in Figure 23 & 24 compare mean and Standard Deviation for different values of particles/sec and for a 0.4-meter grid resolution. Interestingly, the mean has more noise at lower values of particles/s and a smooth curve at higher values of particle/s. The same is reflected in the plots of Standard Deviation; values of the Standard Deviation are higher for 100 particles/sec and lower for 30000 particles/sec. This suggests that the variability in mass flux is inversely proportional to the particle insertion rate.

The Standard Deviation of the line of cells passing through the center of the floor can also be used to compare across different grid sizes. Figures 25 and 26 compare the mean and Standard Deviation across all the gird sizes for fixed particle insertion rates. It is worth noting that the variability of the mass flux is inversely proportional to the grid cell size.

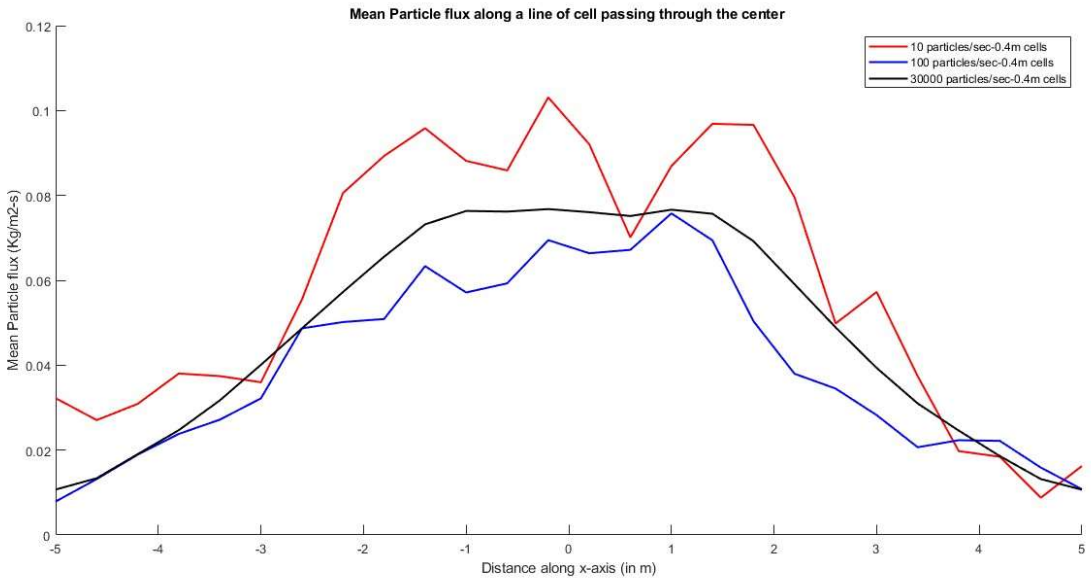

Figure 23: Comparison of mean of particle mass flux with varying particle injection rates and a 0.4-meter grid cell configuration.

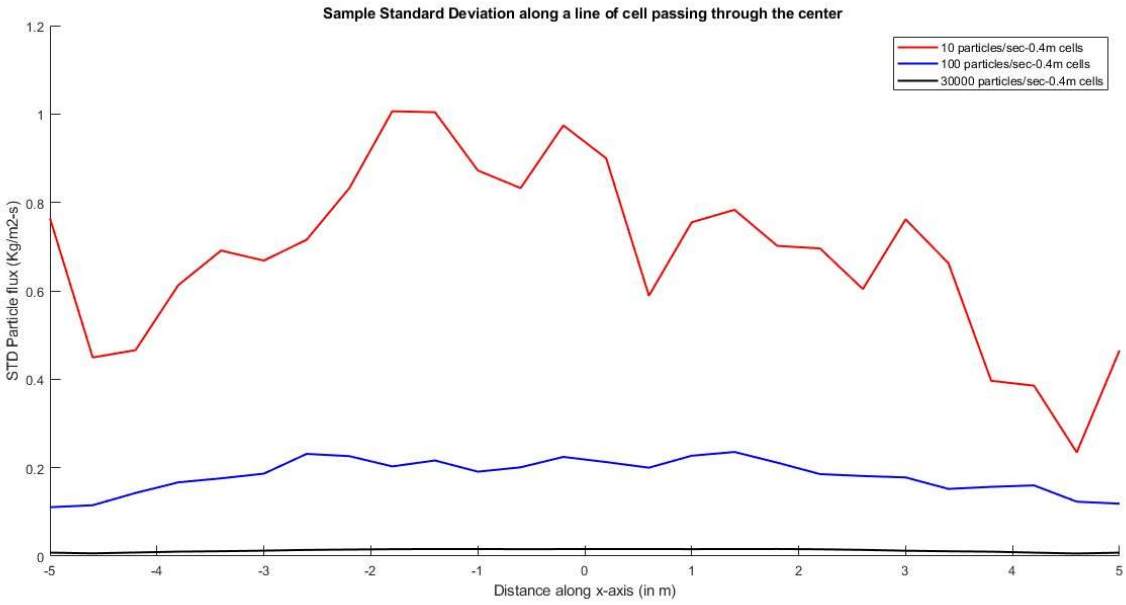

Figure 24: Comparison of Sample Standard Deviation of particle mass flux with varying particle injection rates in a 0.4-meter grid cell configuration

Another way of comparing the variability between test cases is by averaging the Standard Deviation by the number of cells on the slice.

$$Average\ Standard\ Deviation\ = \frac{Sum\ of\ STD\ value\ of\ all\ grid\ cells}{Total\ number\ of\ grid\ cells}$$

Figure 27 shows the Average Standard Deviation of different grid sizes. It is to be noted that the Average Standard Deviation decreases as the particle insertion rate increases (on a fixed grid size).

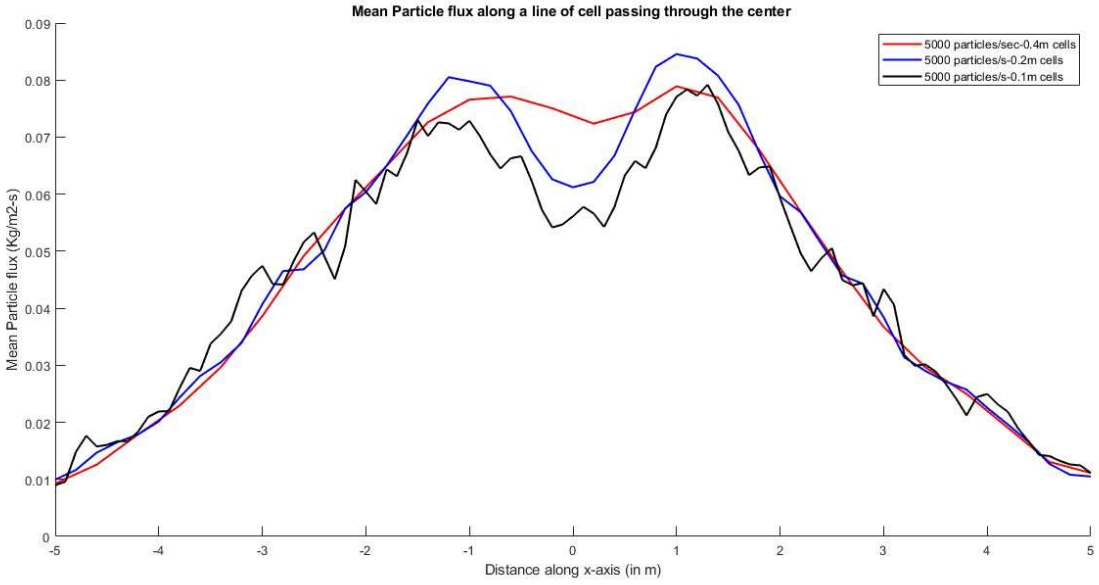

Figure 25: Comparison of mean of particle mass flux with a fixed particle injection rate (at 5000 particles/s) in different grid cell configurations.

Looking at the effect of varying particle injection rate and grid cell size on the variability, a critical inference can be made; the variability of mass flux is inversely proportional to the grid cell size and the particle injection rate.

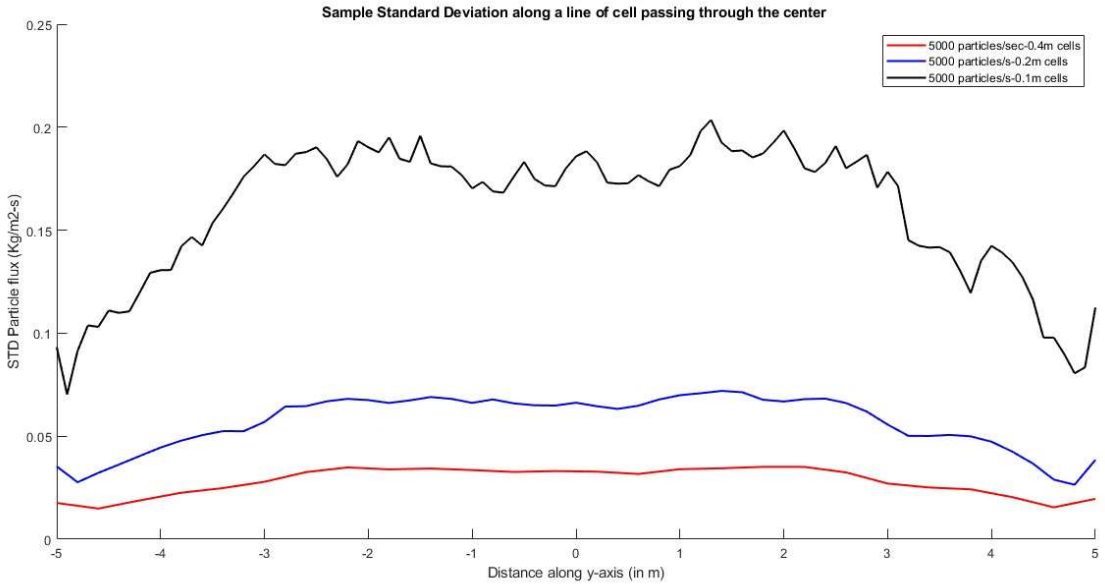

Figure 26: Comparison of mean of particle mass flux with a fixed particle injection rate (at 5000 particles/s) in different grid cell configurations.

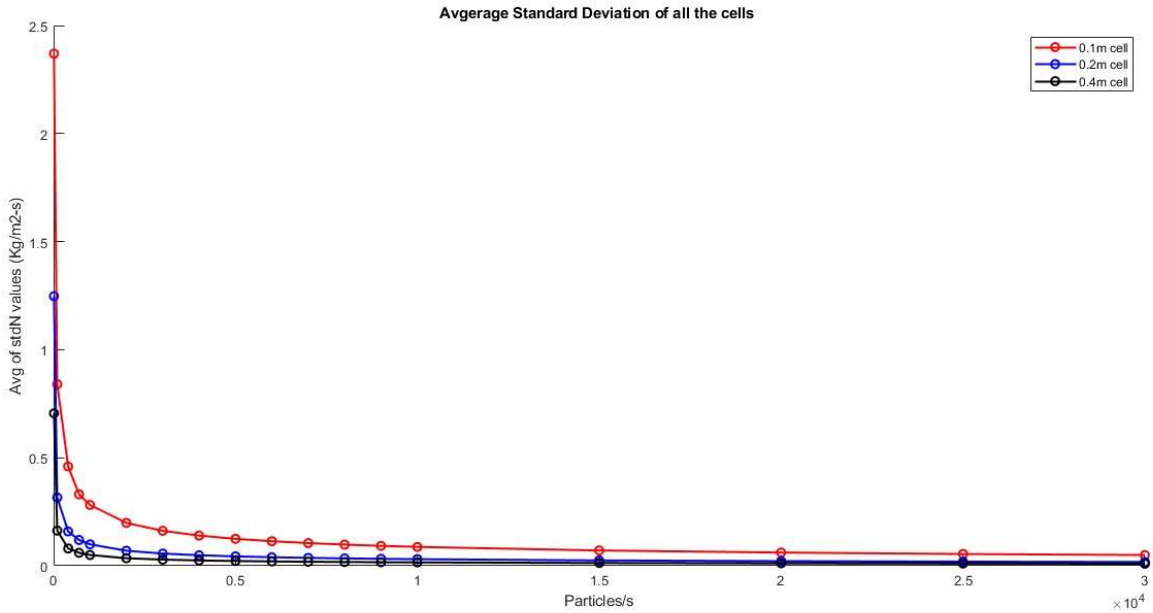

Figure 27: Comparison of mean of particle mass flux with particle injection rate for different choices of grid resolution.

Chapter 9: Revisiting the Hypothesis

Figure 29 shows the mass flux of particles falling on a grid cell with coordinates (x = 2.5 m, y = 5 m) with time. The chosen location (See Figure 28) is suitable for the analysis because it lies at the center of the distance from the wall to the sprinkler and the center of the wall to wall in a perpendicular direction. It can be observed in Figures 29 to 31 that the number of time steps at which no particles are passing through the cell increases as we go from 0.4 m to 0.1 m. Thus the noise increases as we move from 0.4 m to 0.1 m. The relationship between the size of the cell and the number of time steps in which no particle passes through it is depicted in Figure 32.

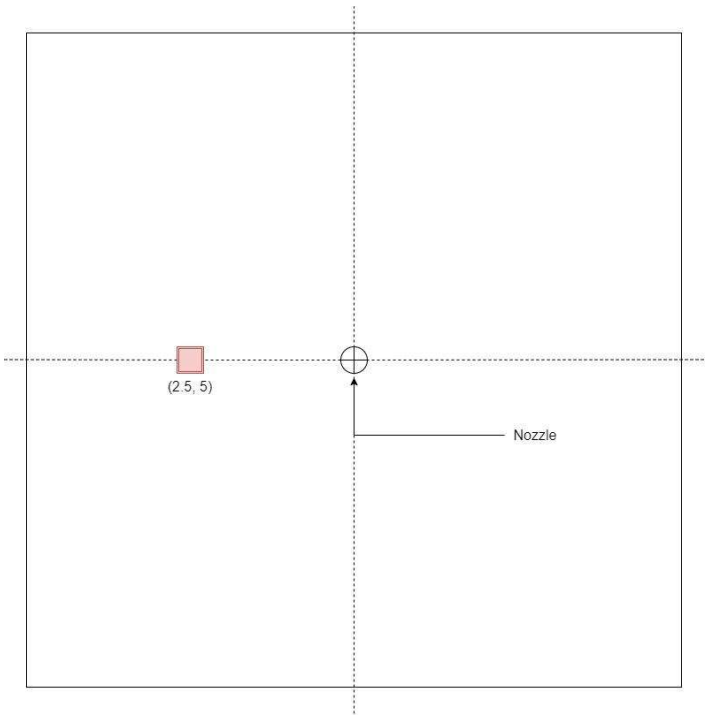

Figure 28: Location of the cell at X=0.25m, Y=5m

Figure 29: Time variations of the mass flux of particles passing through a single cell of 0.1-meter size.

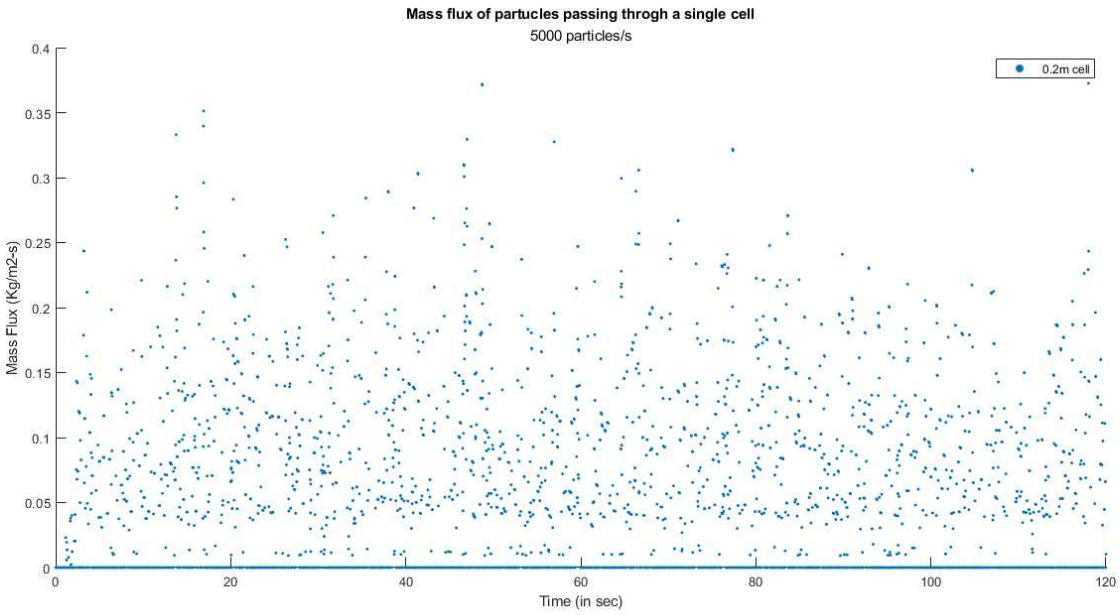

Figure 30: Time variations of the mass flux of particles passing through a single cell of 0.2-meter size.

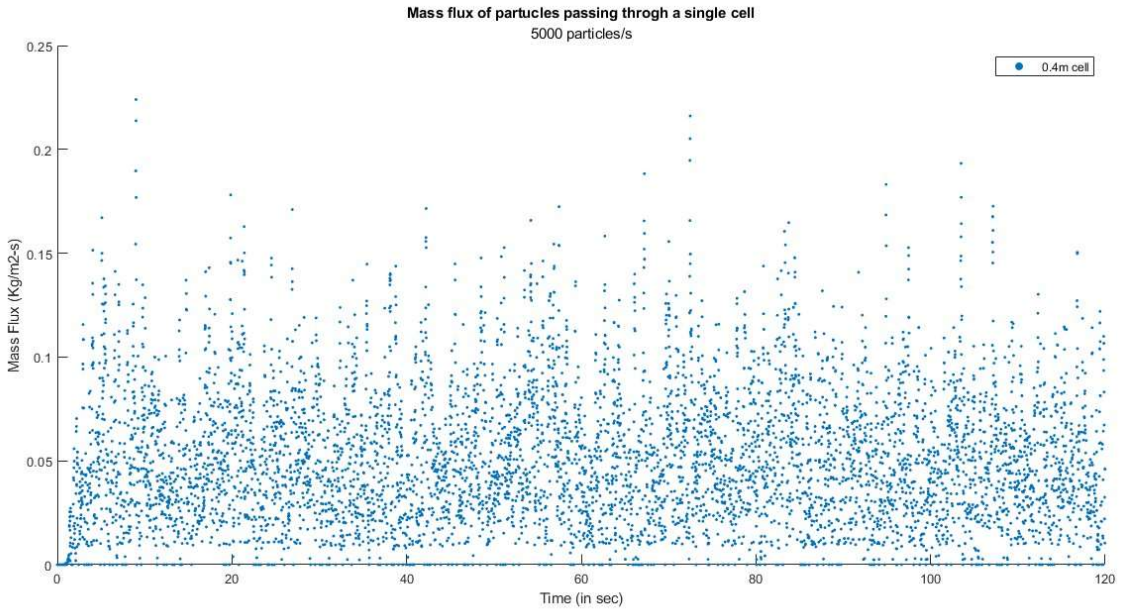

Figure 31: Time variations of the mass flux of particles passing through a single cell of 0.4-meter size.

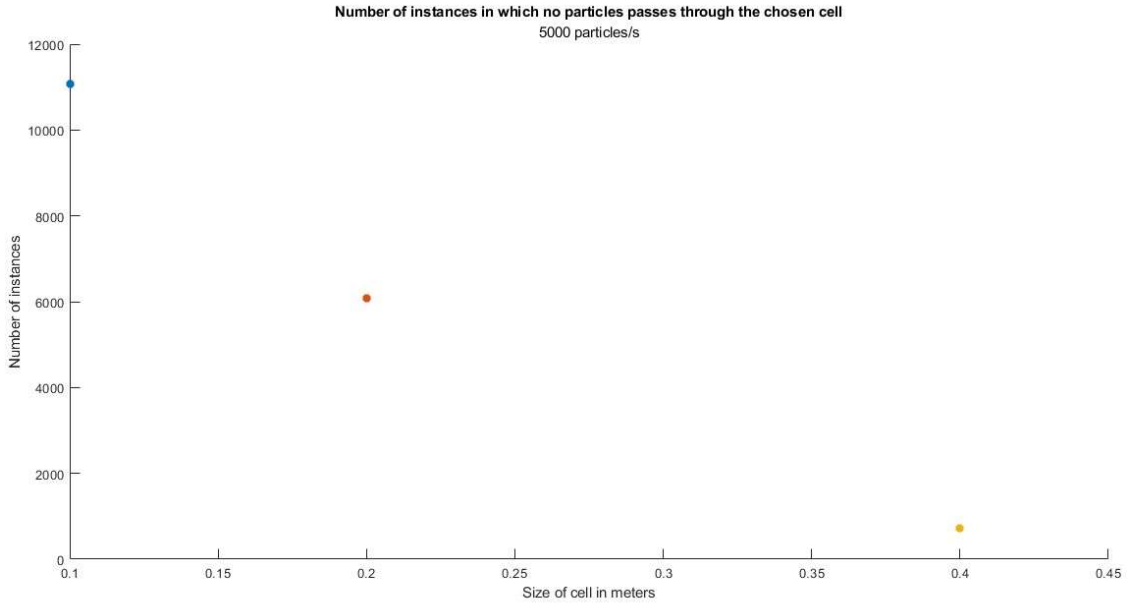

Figure 32: Comparison of the number of instances when no particle passes through the cell with different cell sizes.

Mass flux passing through the cell for the same location was also analysed with varying the particle injection rate (see Figures 33 to 35). It can be observed that the number of time steps at which no particle is passing through the cell decreases as the particle injection rate increases, so much that at 30000 particles per second, there are nearly no time steps at which no particles pass through the cell. The relationship between the particle insertion rate and the number of time steps in which no particle passes through it is depicted in Figure 36.

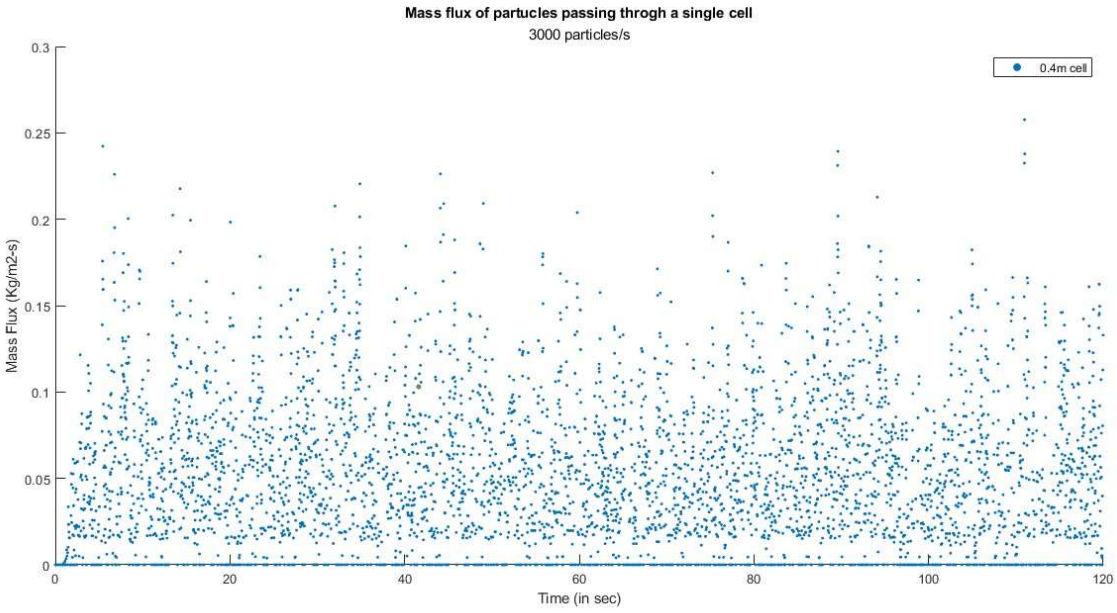

Figure 33: Time variations of the mass flux of particles passing through a single cell of 0.4-meter size at 3000 particle/s.

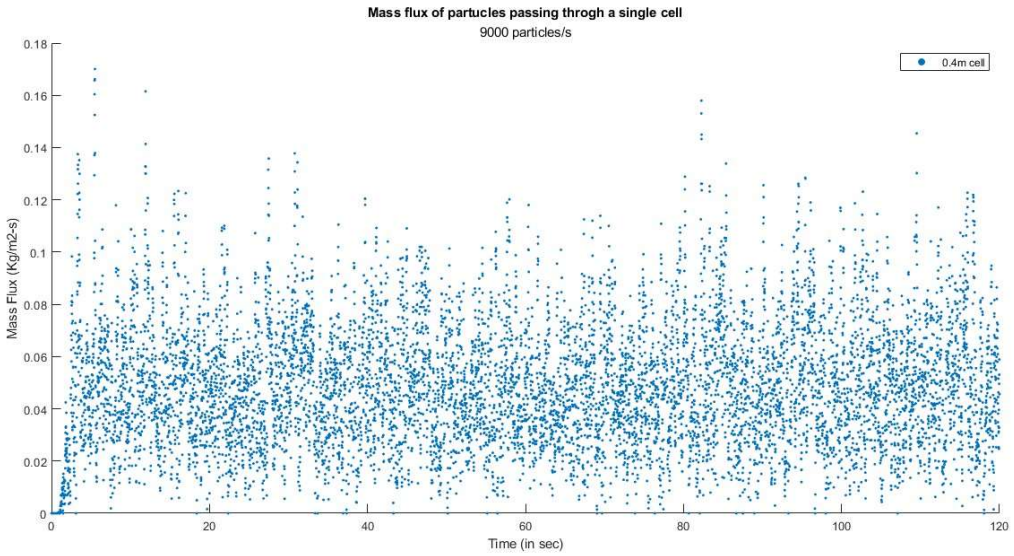

Figure 34: Time variations of the mass flux of particles passing through a single cell of 0.4-meter size at 9000 particle/s.

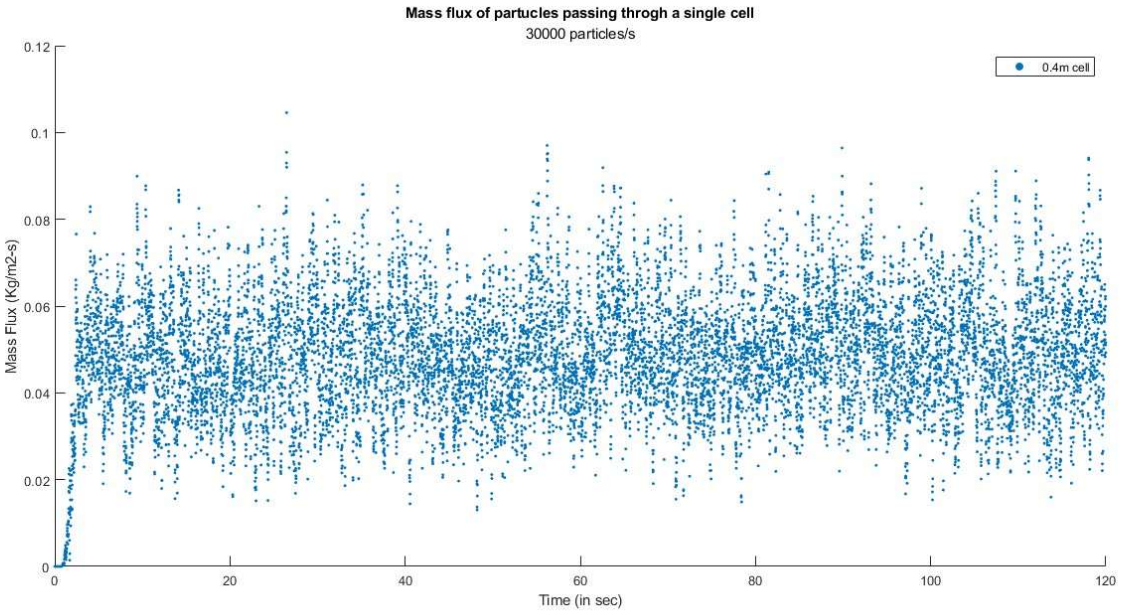

Figure 35: Time variations of the mass flux of particles passing through a single cell of 0.4-meter size at 30000 particle/s.

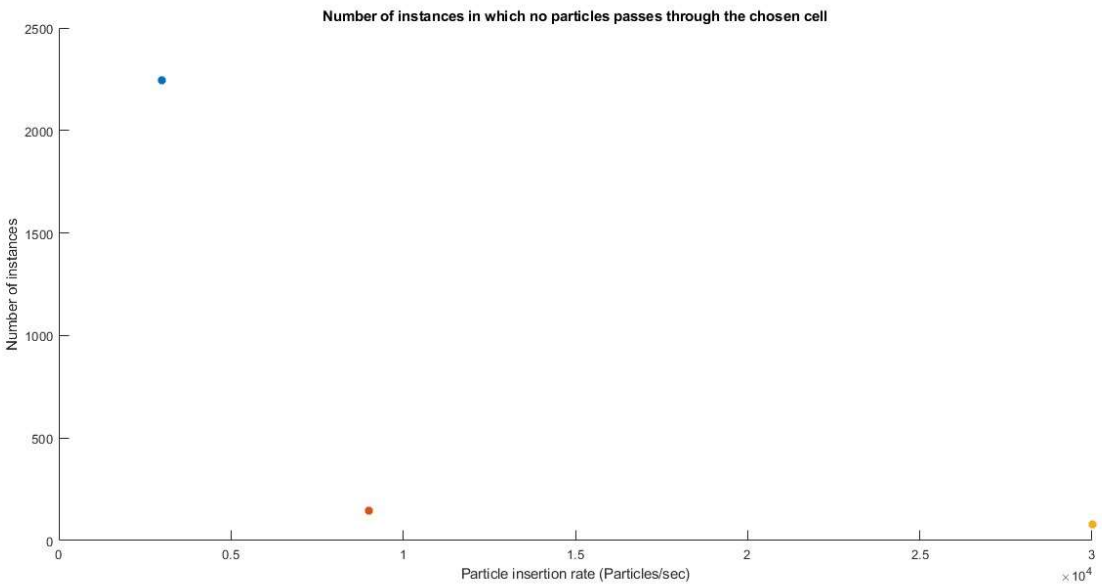

Figure 36: Comparison of the number of instances when no particle passes through the cell with different particle insertion rates.

Chapter 10: Simulation with a Fire

10.1 Analysis with Fire

Three simulations, at 3000 particles/s with 0.4-meter resolution, 9000 particles/s with 0.2-meter resolution and 30000 particle/s with 0.1-meter resolution, were run with fire at the center and offset from the center of the nozzle as shown in Figures 38 to 40.

The fire was set up to burn at 1 MW. Figure 37 confirms that the heat release rate output was as prescribed.

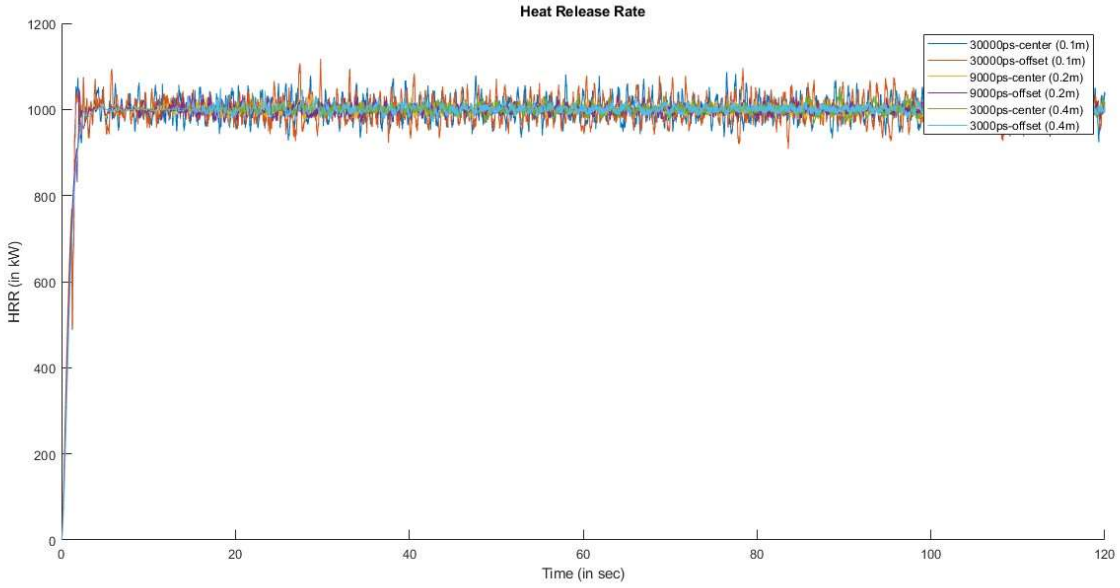

Figure 37: Heat release rate for simulations with fire.

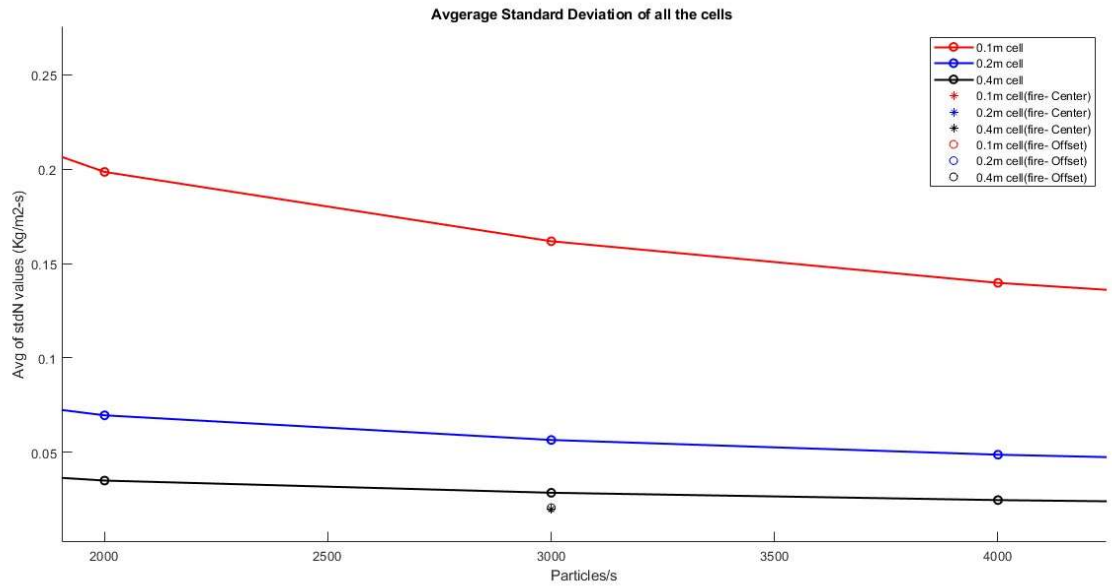

Figure 38: Average Sample Standard Deviation of 3000 particle/s with 0.4 meters cell size compared to the values without fire data.

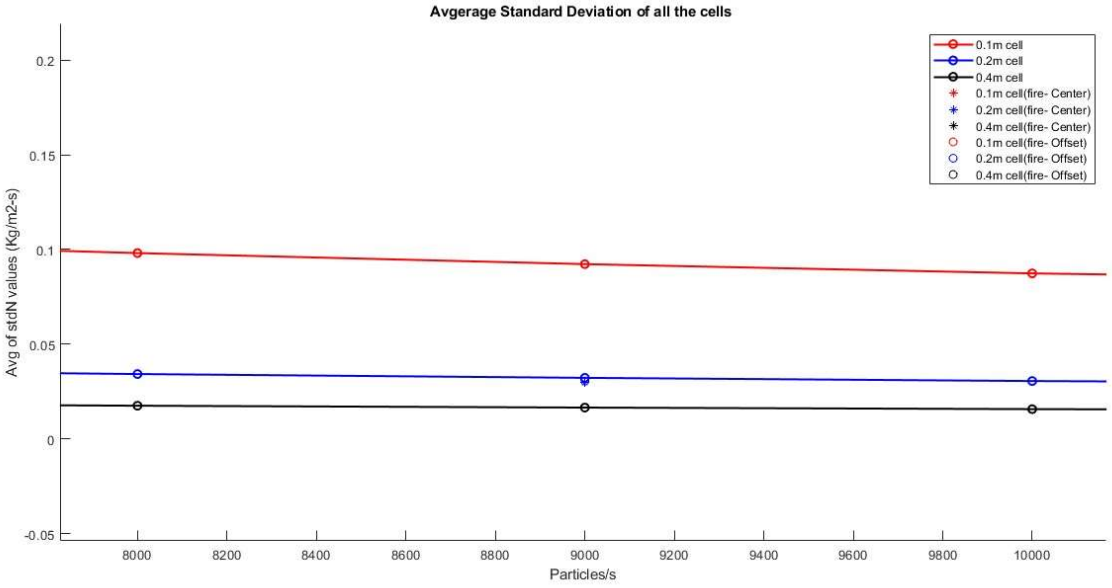

Figure 39: Average Sample Standard Deviation of 9000 particle/s with 0.2 meters cell size compared to the values without fire data.

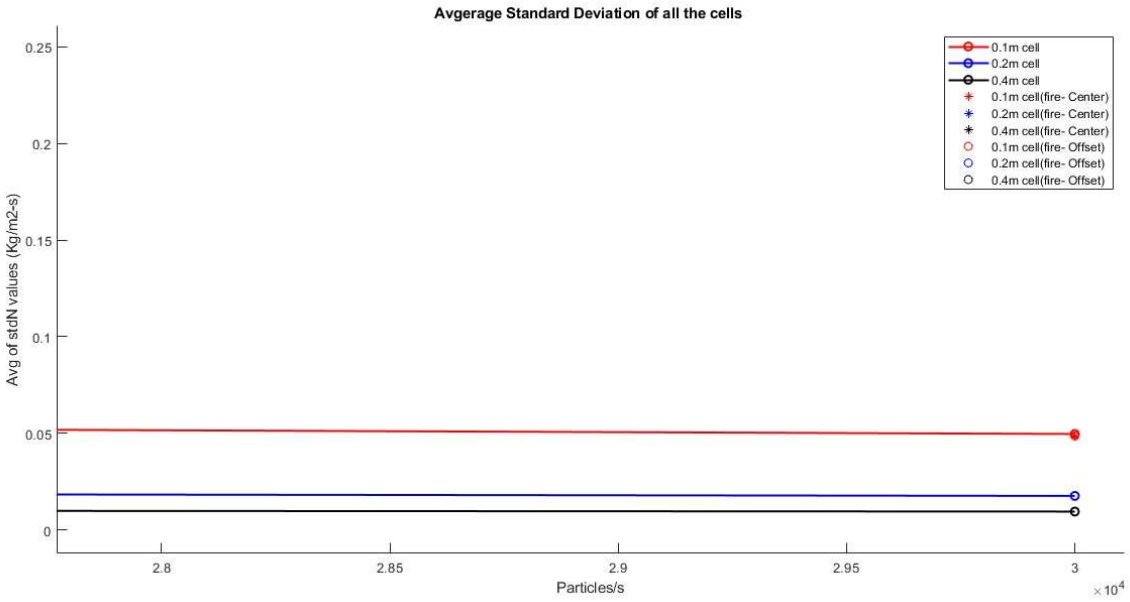

Figure 40: Average Sample Standard Deviation of 30000 particle/s with 0.1 meters cell size compared to the values without fire data.

It can be noted that the new data points (with fire) are very close to the points belonging to the setting without fire, and hence the relationship between variability and particle injection rate withholds.

The mentioned relationship can also be verified by plotting the standard deviation for a line of cells passing through the center of the fire. Figures 41 to 44 present the comparison of the mean and Sample Standard Deviation of the mass flux along the line of the cells passing through the center of the fire. It is worth noting that the curves look very similar, except that there is a dip at the location of the fire because water droplets are not able to reach the fire and drift away because of the vertical buoyant flow.

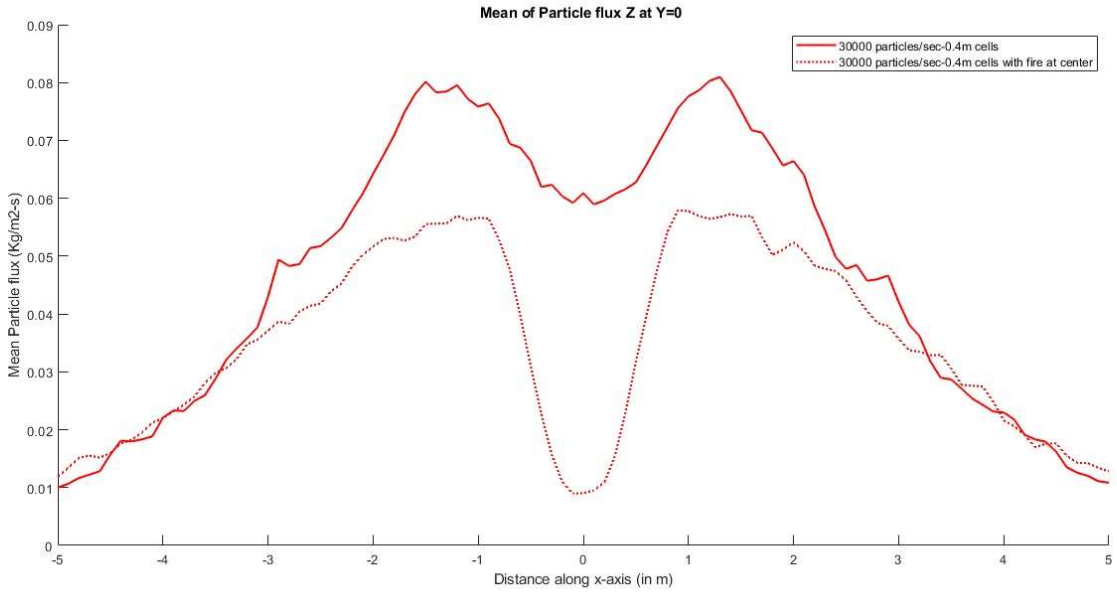

Figure 41: Comparison of the mean of particle flux without fire and with fire at the center.

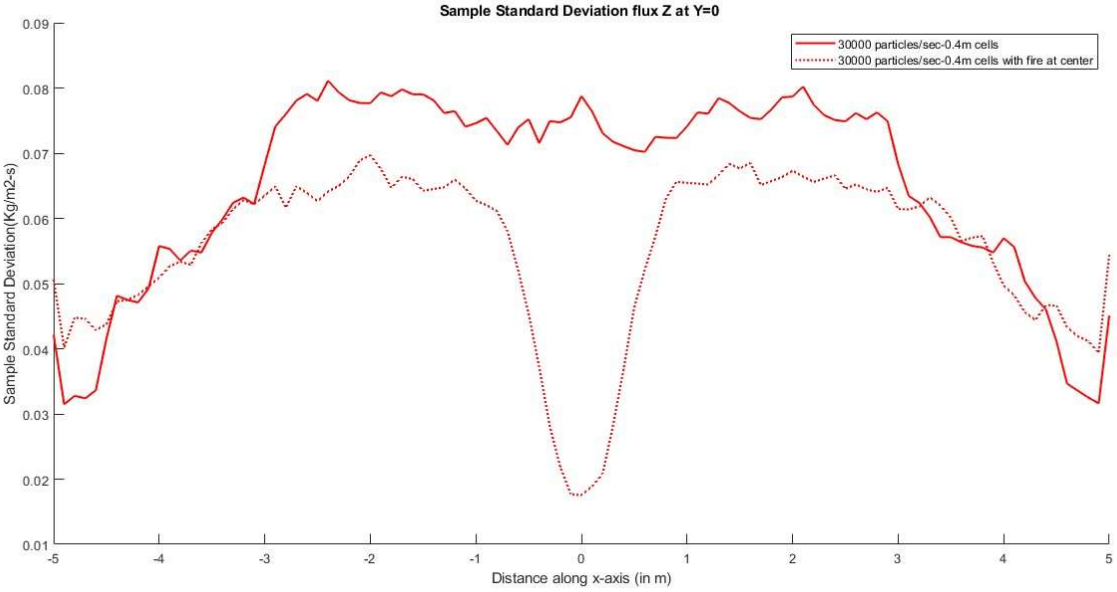

Figure 42: Comparison of the Sample Standard Deviation of particle flux without fire and with fire at the center.

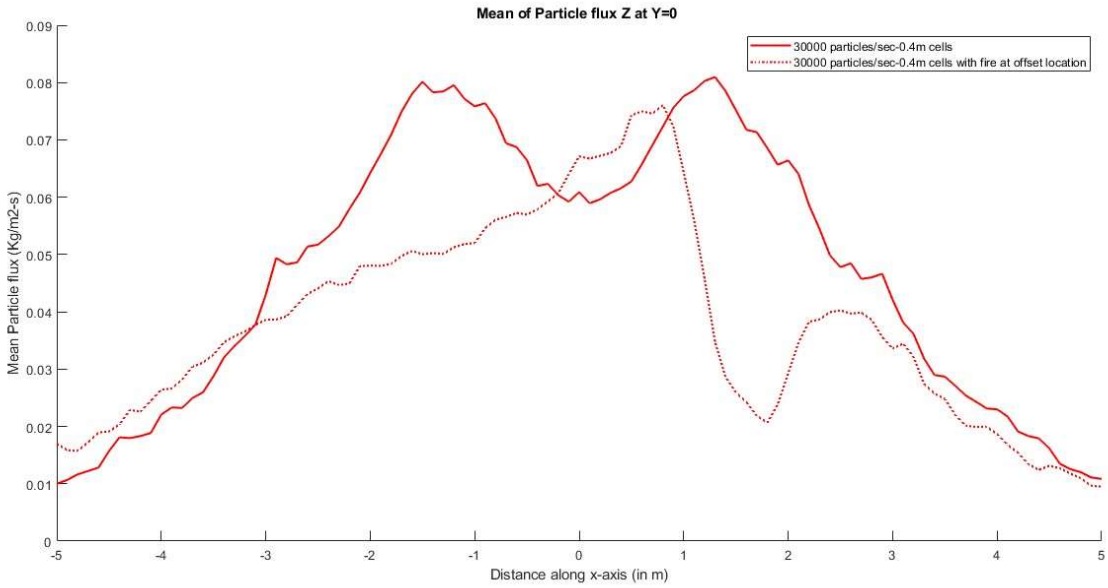

Figure 43: Comparison of the mean of particle flux without fire and with offset fire.

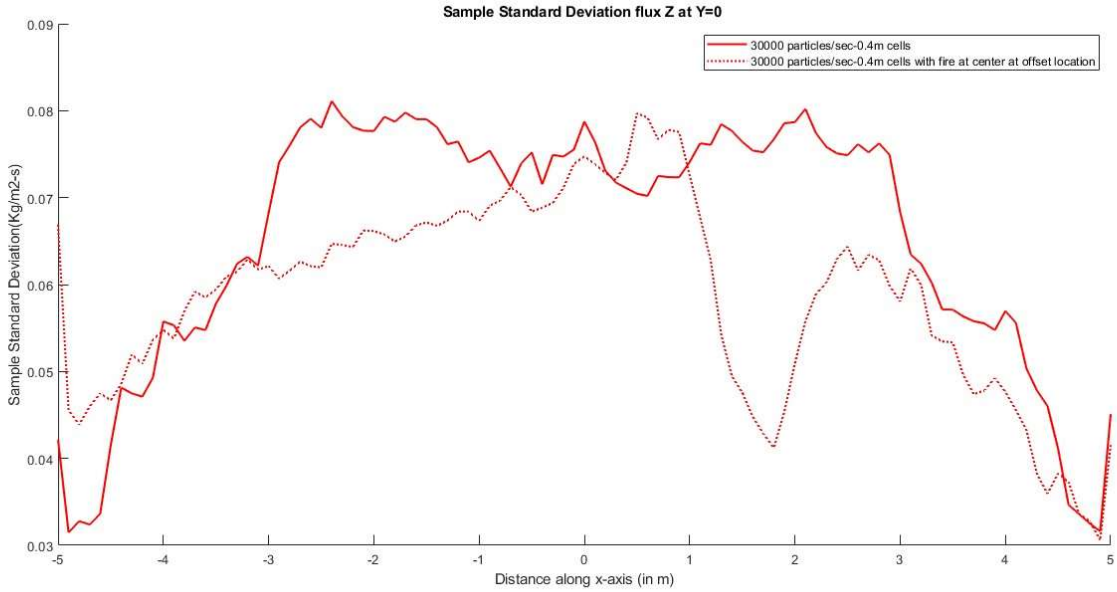

Figure 44: Comparison of Sample Standard Deviation of particle flux without fire and with offset fire.

10.2 Analysing with 'e_coefficient'

FDS offers a model to mimic the suppression of fire by water by using the E_COEFFICIENT parameter[1].

To account for fire suppression by water in simulations, FDS uses an exponential function to characterize the reduction of the pyrolysis rate. This reduction is a result of water impinging on the fuel surface, cooling it, and modifying the chemical reactions, which ultimately leads to lower fuel pyrolysis and burning rates.

The local mass loss rate of the fuel is expressed in the form:

$$\dot{m}''_f(t) = \dot{m}''_{f,0}(t)e^{-\int k(t)dt}$$

A user-specified burning rate per unit area, $\dot{m}''_{f,0}(t)$, is assumed when water is not applied, and the local water mass per unit area, $\dot{m}''_w$, in units of kg/m2, is used to determine the function k.

$$k(t) = E_COEFFI\dot{C}IENT \times m''_{\mathrm{w}}(t)$$

Additional simulations were also run (including this model) to check how changing the particle injection rate affects this model. Figure 45 shows the heat release rate curves for the simulations using the E_COEFFICIENT model. It is worth noting the curves are very consistent with the change in the particle injection rate. The heat release rate starts to decrease after the nozzle is activated (at t = 7 seconds).

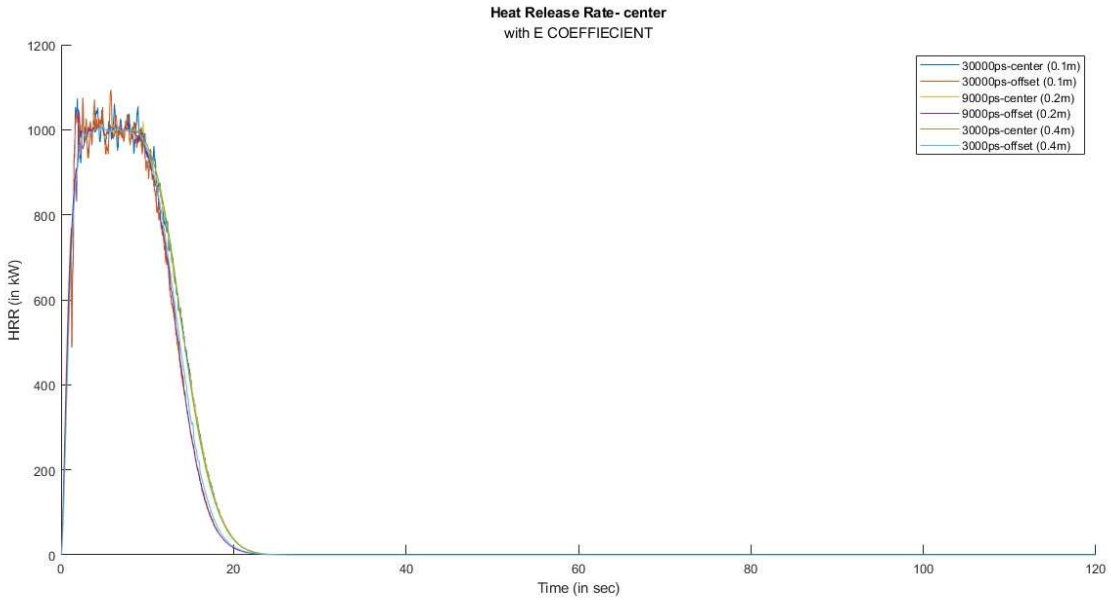

Figure 45: Comparison of the time variations of the heat release rate for different values of the particle injection rate.

More simulations were run to understand the impact of lower values of the particle injection rate on the fire suppression model. Figure 46 shows the heat release rate curves for lower values of the particle injection rate and for a 0.4-meter grid resolution. Even when the injection rate is as high as 10 particles per second, the heat release rate still displays the expected trend, albeit with some fluctuations. This is primarily because the injection rate may vary, but the mass of water represented by each 'superdrop' remains constant, which is equivalent to a flow rate of 180 liters per minute. Thus, even though there may be more or fewer particles injected at any given time, the overall amount of water in the system remains consistent, allowing the heat release rate to follow the expected pattern.

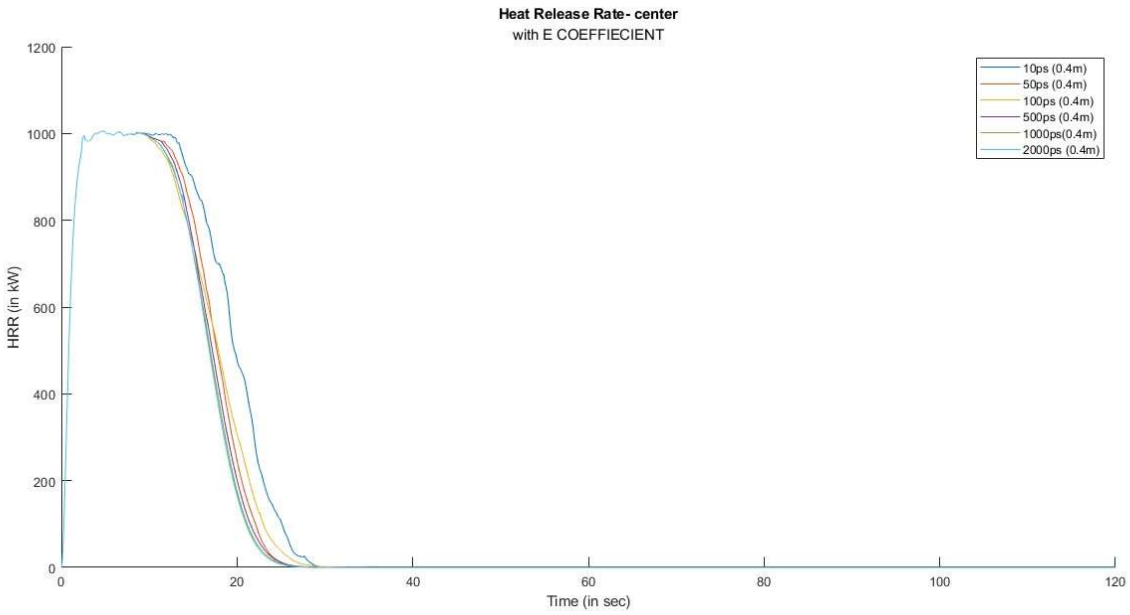

Figure 46: Comparison of the time variations of the heat release rate for different values of the particle injection rate.

Chapter 11: Conclusion- Particles Project

11.1 Conclusion

It can be said with certainty, based on the analysis of data from the simulations, that the variability of mass flux in z direction is inversely proportional to the particle insertion rate and grid cell size. However, the scaling relationship is yet to be established.

When conducting a simulation, it's crucial to minimize the impact of variability to ensure accurate results. To achieve this, there are two primary steps to follow.

The first step is to determine the appropriate size of the grid. This decision should be based on various factors, including the project's requirements, computation cost, domain size, and how the results will be used and processed. Finer grid size improves accuracy but increases computational cost due to smaller time steps dictated by the (Courant-Friedrichs-Lewy) CFL condition in FDS. A coarser grid size reduces computational cost but may lead to reduced accuracy due to a lack of detail in simulations. Choosing an appropriate grid size in FDS involves a trade-off between accuracy and computational cost. Grid sensitivity studies can help identify the optimal grid size for the desired level of accuracy and available computational resources by comparing the resulting accuracy and computational cost with varying grid sizes.

Once the appropriate grid size has been determined, the second step is to select the particle injection rate. It's essential to choose this rate carefully, as the default rate may not be appropriate for a smaller grid size. To determine the best injection rate, a

trial run can be conducted with default settings, and diagnostics can be used to capture the mass flux. This information can then be used to adjust the injection rate accordingly.

Also, the simulations that utilize the E_COEFFICIENT for fire suppression are not affected by changes in the particle insertion rate in this particular setting of heat release rate and sprinkler characteristics.

11.2 Future Work

The data from the simulations could be used to establish a relationship between the variability, particle injection rate and grid cell size, if required more simulations could be run. With a quantitative relationship between the three parameters, it will be possible to be sure if the default rate of 5000 particles/sec is good enough for a given grid cell size. The relationship would also be able to establish what particle injection rate is suitable for a given grid cell size.

Performing more tests with E_COEFFICIENT, while varying heat release rates and sprinkler characteristics, can help to better understand how particle injection rates affect the surface wetting suppression model.

Appendix A: Using RAMP in FDS

```
&HEAD CHID='simple_ramp', TITLE='simple fire ramp - ultra
fast'  /

&MESH  IJK=50,50,30,  XB=-2.5,2.5,-2.5,2.5,0.0,3.0  /  75k
cells

&TIME T_END=75.0 /

&REAC ID='POLYURETHANE_GM27',
      FYI='SFPE Handbook, GM27',
      FUEL='REAC_FUEL',
      C=1.0,
      H=1.7,
      O=0.3,
      N=0.08,
      CO_YIELD=0.042,
      SOOT_YIELD=0.198/

&SURF    ID='BURNER',    HRRPUA=1055,    RAMP_Q='tsquared'
COLOR='RED' /
&OBST XB= -0.5, 0.5, -0.5, 0.5, 0.0, 0.1, /
&VENT XB= -0.5, 0.5, -0.5, 0.5, 0.1, 0.1, SURF_ID='BURNER'
     /

&RAMP ID='tsquared',     T=   0    ,    F=   0    /
&RAMP ID='tsquared',     T=   1    ,    F=   0.000177778
     /
&RAMP ID='tsquared',     T=   2    ,    F=   0.000711111
     /
&RAMP ID='tsquared',     T=   3    ,    F=   0.0016    /
&RAMP ID='tsquared',     T=   4    ,    F=   0.002844444
     /
&RAMP ID='tsquared',     T=   5    ,    F=   0.004444444
     /
&RAMP ID='tsquared',     T=   6    ,    F=   0.0064    /
&RAMP ID='tsquared',     T=   7    ,    F=   0.008711111
     /
&RAMP ID='tsquared',     T=   8    ,    F=   0.011377778
     /
&RAMP ID='tsquared',     T=   9    ,    F=   0.0144    /
&RAMP ID='tsquared',     T=   10   ,    F=   0.017777778
     /
```

```
&RAMP ID='tsquared',     T=   11   ,    F=   0.021511111
     /
&RAMP ID='tsquared',     T=   12   ,    F=   0.0256    /
&RAMP ID='tsquared',     T=   13   ,    F=   0.030044444
     /
&RAMP ID='tsquared',     T=   14   ,    F=   0.034844444
     /
&RAMP ID='tsquared',     T=   15   ,    F=   0.04 /
&RAMP ID='tsquared',     T=   16   ,    F=   0.045511111
     /
&RAMP ID='tsquared',     T=   17   ,    F=   0.051377778
     /
&RAMP ID='tsquared',     T=   18   ,    F=   0.0576    /
&RAMP ID='tsquared',     T=   19   ,    F=   0.064177778
     /
&RAMP ID='tsquared',     T=   20   ,    F=   0.071111111
     /
&RAMP ID='tsquared',     T=   21   ,    F=   0.0784    /
&RAMP ID='tsquared',     T=   22   ,    F=   0.086044444
     /
&RAMP ID='tsquared',     T=   23   ,    F=   0.094044444
     /
&RAMP ID='tsquared',     T=   24   ,    F=   0.1024    /
&RAMP ID='tsquared',     T=   25   ,    F=   0.111111111
     /
&RAMP ID='tsquared',     T=   26   ,    F=   0.120177778
     /
&RAMP ID='tsquared',     T=   27   ,    F=   0.1296    /
&RAMP ID='tsquared',     T=   28   ,    F=   0.139377778
     /
&RAMP ID='tsquared',     T=   29   ,    F=   0.149511111
     /
&RAMP ID='tsquared',     T=   30   ,    F=   0.16 /
&RAMP ID='tsquared',     T=   31   ,    F=   0.170844444
     /
&RAMP ID='tsquared',     T=   32   ,    F=   0.182044444
     /
&RAMP ID='tsquared',     T=   33   ,    F=   0.1936    /
&RAMP ID='tsquared',     T=   34   ,    F=   0.205511111
     /
&RAMP ID='tsquared',     T=   35   ,    F=   0.217777778
     /
&RAMP ID='tsquared',     T=   36   ,    F=   0.2304    /
&RAMP ID='tsquared',     T=   37   ,    F=   0.243377778
     /
&RAMP ID='tsquared',     T=   38        F=   0.256711111
     /
```

```
&RAMP ID='tsquared',     T=   39         F=   0.2704    /
&RAMP ID='tsquared',     T=   40         F=   0.284444444
     /
&RAMP ID='tsquared',     T=   41         F=   0.298844444
     /
&RAMP ID='tsquared',     T=   42         F=   0.3136    /
&RAMP ID='tsquared',     T=   43         F=   0.328711111
     /
&RAMP ID='tsquared',     T=   44         F=   0.344177778
     /
&RAMP ID='tsquared',     T=   45         F=   0.36 /
&RAMP ID='tsquared',     T=   46         F=   0.376177778
     /
&RAMP ID='tsquared',     T=   47         F=   0.392711111
     /
&RAMP ID='tsquared',     T=   48         F=   0.4096    /
&RAMP ID='tsquared',     T=   49         F=   0.426844444
     /
&RAMP ID='tsquared',     T=   50         F=   0.444444444
     /
&RAMP ID='tsquared',     T=   51         F=   0.4624    /
&RAMP ID='tsquared',     T=   52         F=   0.480711111
     /
&RAMP ID='tsquared',     T=   53         F=   0.499377778
     /
&RAMP ID='tsquared',     T=   54         F=   0.5184    /
&RAMP ID='tsquared',     T=   55         F=   0.537777778
     /
&RAMP ID='tsquared',     T=   56         F=   0.557511111
     /
&RAMP ID='tsquared',     T=   57         F=   0.5776    /
&RAMP ID='tsquared',     T=   58         F=   0.598044444
     /
&RAMP ID='tsquared',     T=   59         F=   0.618844444
     /
&RAMP ID='tsquared',     T=   60         F=   0.64 /
&RAMP ID='tsquared',     T=   61         F=   0.661511111
     /
&RAMP ID='tsquared',     T=   62         F=   0.683377778
     /
&RAMP ID='tsquared',     T=   63         F=   0.7056    /
&RAMP ID='tsquared',     T=   64         F=   0.728177778
     /
&RAMP ID='tsquared',     T=   65         F=   0.751111111
     /
&RAMP ID='tsquared',     T=   66         F=   0.7744    /
```

```
&RAMP ID='tsquared',     T=   67        F=   0.798044444
     /
&RAMP ID='tsquared',     T=   68        F=   0.822044444
     /
&RAMP ID='tsquared',     T=   69        F=   0.8464    /
&RAMP ID='tsquared',     T=   70        F=   0.871111111
     /
&RAMP ID='tsquared',     T=   71        F=   0.896177778
     /
&RAMP ID='tsquared',     T=   72        F=   0.9216    /
&RAMP ID='tsquared',     T=   73        F=   0.947377778
     /
&RAMP ID='tsquared',     T=   74        F=   0.973511111
     /
&RAMP ID='tsquared',     T=   75        F=   1    /

&VENT MB='ZMIN',SURF_ID='OPEN' /
&VENT MB='ZMAX',SURF_ID='OPEN' /
&VENT MB='YMIN',SURF_ID='OPEN' /
&VENT MB='YMAX',SURF_ID='OPEN' /
&VENT MB='ZMIN',SURF_ID='OPEN' /
&VENT MB='ZMAX',SURF_ID='OPEN' /

&TAIL /
```

Appendix B: Using SPREAD_RATE in FDS

```
&HEAD CHID='spread_rate', TITLE='Simple spread rate'  /

&MESH  IJK=50,50,30,  XB=-2.5,2.5,-2.5,2.5,0.0,3.0  /  75k
cells

&TIME T_END=75.0 /

&REAC ID='POLYURETHANE_GM27',
      FYI='SFPE Handbook, GM27',
      FUEL='REAC_FUEL',
      C=1.0,
      H=1.7,
      O=0.3,
      N=0.08,
      CO_YIELD=0.042,
      SOOT_YIELD=0.198/

&SURF ID='BURNER', HRRPUA=1055, COLOR='RED' /
&OBST XB= -0.5, 0.5, -0.5, 0.5, 0.0, 0.1, /
&VENT XB= -0.5, 0.5, -0.5, 0.5, 0.1, 0.1, SURF_ID='BURNER',
SPREAD_RATE=0.007522527781    /

&VENT MB='ZMIN',SURF_ID='OPEN' /
&VENT MB='ZMAX',SURF_ID='OPEN' /
&VENT MB='YMIN',SURF_ID='OPEN' /
&VENT MB='YMAX',SURF_ID='OPEN' /
&VENT MB='ZMIN',SURF_ID='OPEN' /
&VENT MB='ZMAX',SURF_ID='OPEN' /

&TAIL /
```

Appendix C: Alternate Method to Place Observer

Overview

You want to create a viewpoint that is in a specific location and at a specific orientation in the PyroSim Results Viewer. The specifications appear to be a JSON array.

Solution

1. If it does not already exist, create a file named "[SIMULATIONNAME].views" within the folder that contains the FDS results.
    a. [SIMULATIONNAME] is the name of the FDS simulation – it should be the same as the FDS results files and SMV file.
    b. TIP: If you want to apply the same viewpoint to multiple versions of the simulation, create the viewpoint in PyroSim Results Viewer for one simulation and then copy / paste the ".views" file (renaming as indicated above) to the folders of the other simulations.
2. Open the file using a text editor and either edit the existing text or edit the text below and copy / paste into the file. TODO: determine what each value corresponds to in PyroSim.


```
[{
"name":"Default",
"state":{
```

"loc":[10.601689338109455,4.199558936236595,1.612899588408769],
"ref":[11.598380339772664,4.207329622440867,1.5319881328570082],
"far":8.071210757625737,
"zoom":1.0,
"up":[0.08090899655538651,6.308057585403541E-4,0.996721293221177],
"near":0.004729561625939311,
"zoomloc":[0.0,0.0],
"fov":0.7853981633974483
},
"type":"camera_view"
}]

3. Save the edits to the ".views" file and then open the ".smv" file with PyroSim Results Viewer.
    a. The viewpoint name, "[FDS] " + [name from above], should appear under "Views" -> "Viewpoints"

Appendix D: Using ‘slread.m’ to Read Slice Files

```
% Reading slice files- 0.1m cell
[T_10_p1,      Time_10_p1]    =slread(   '10ps_1_8_p1.sf',      0,120);
[T_100_p1,     Time_100_p1]   =slread(   '100ps_1_8_p1.sf',     0,120);
[T_400_p1,     Time_400_p1]   =slread(   '400ps_1_8_p1.sf',     0,120);
[T_700_p1,     Time_700_p1]   =slread(   '700ps_1_8_p1.sf',     0,120);
[T_1000_p1,    Time_1000_p1]  =slread(   '1000ps_1_8_p1.sf',    0,120);
[T_2000_p1,    Time_2000_p1]  =slread(   '2000ps_1_8_p1.sf',    0,120);
[T_3000_p1,    Time_3000_p1]  =slread(   '3000ps_1_8_p1.sf',    0,120);
[T_4000_p1,    Time_4000_p1]  =slread(   '4000ps_1_8_p1.sf',    0,120);
[T_5000_p1,    Time_5000_p1]  =slread(   '5000ps_1_8_p1.sf',    0,120);
[T_6000_p1,    Time_6000_p1]  =slread(   '6000ps_1_8_p1.sf',    0,120);
[T_7000_p1,    Time_7000_p1]  =slread(   '7000ps_1_8_p1.sf',    0,120);
[T_8000_p1,    Time_8000_p1]  =slread(   '8000ps_1_8_p1.sf',    0,120);
[T_9000_p1,    Time_9000_p1]  =slread(   '9000ps_1_8_p1.sf',    0,120);
[T_10000_p1,   Time_10000_p1] =slread(   '10000ps_1_8_p1.sf',   0,120);
[T_15000_p1,   Time_15000_p1] =slread(   '15000ps_1_8_p1.sf',   0,120);
[T_20000_p1,   Time_20000_p1] =slread(   '20000ps_1_8_p1.sf',   0,120);
[T_25000_p1,   Time_25000_p1] =slread(   '25000ps_1_8_p1.sf',   0,120);
[T_30000_p1,   Time_30000_p1] =slread(   '30000ps_1_8_p1.sf',   0,120);
```

Bibliography

[1] McGrattan, K. , McDermott, R. , Weinschenk, C. and Forney, G. (2013), Fire Dynamics Simulator Users Guide, Sixth Edition, Special Publication (NIST SP), National Institute of Standards and Technology, Gaithersburg, MD, [online], https://doi.org/10.6028/NIST.sp.1019 (Accessed April 6, 2023)

[2] Hurley, M. J., Gottuk, D. T., Hall, J. J. R., Harada, K., Kuligowski, E. D., Puchovsky, M., Torero, J. L., Watts, J. J. M., & Wieczorek, C. J. (Eds.). (2015). *SFPE handbook of fire protection engineering*. Springer New York.

[3] Kuligowski, E. D., Gwynne, S. M. V., Kinsey, M. J., & Hulse, L. (2017). Guidance for The model user on representing human behavior in egress models. *Fire Technology*, *53*(2), 649–672. https://doi.org/10.1007/s10694-016-0586-2

[4] Quintiere, J. G. (2006). *Fundamentals of fire phenomena*. John Wiley. https://doi.org/10.1002/0470091150

[5] D. Canter, Fires and human behaviour: Emerging issues, Fire Safety Journal, Volume 3, Issue 1, 1980, Pages 41-46, ISSN 0379-7112, https://doi.org/10.1016/0379-7112(80)90006-5.

[6] Kuligowski, E. D., & United States. National Bureau of Standards. (2009). *The process of human behavior in fires* (Ser. Nist technical note, 1632). U.S. Dept. of Commerce, National Institute of Standards and Technology. Retrieved March 21, 2023.

[7] Kinsey, M. J., Gwynne, S. M. V., Kuligowski, E. D., & Kinateder, M. (2019). Cognitive biases within decision making during fire evacuations. *Fire Technology*, *55*(2), 465–485. https://doi.org/10.1007/s10694-018-0708-0

[8] Bryan, J. L., Center for Fire Research (U.S.), & University of Maryland. Fire Protection Curriculum. (1977). Smoke as a determinant of human behavior in fire situations (project people). University of Maryland, College of Engineering, Fire Protection Curriculum.

[9] Tzani, M., Besharat, J., Charalampous, V., & Stylios, C. (2020, September). Building a Virtual Reality Fire Environment based on Fire Dynamic Simulator. *2020 International Conference on Information Technologies (InfoTech)*. https://doi.org/10.1109/infotech49733.2020.9211048

[10] Z. Xu, X.Z. Lu, H. Guan, C. Chen, A.Z. Ren, A virtual reality based fire training simulator with smoke hazard assessment capacity, Advances in Engineering Software, Volume 68, 2014, Pages 1-8, ISSN 0965-9978, https://doi.org/10.1016/j.advengsoft.2013.10.004

[11] Zalok, E., Hadjisophocleous, G.V. Assessment of the Use of Fire Dynamics Simulator in Performance-Based Design. *Fire Technol* **47**, 1081–1100 (2011). https://doi.org/10.1007/s10694-009-0117-5

[12] Thunderhead Engineering. (n.d.). PyroSim. Retrieved April 2, 2023, from https://www.thunderheadeng.com/pyrosim

[13] Vytenis Babrauskas, Richard D. Peacock, Heat release rate: The single most important variable in fire hazard, Fire Safety Journal, Volume 18, Issue 3, 1992,

Pages 255-272, ISSN 0379-7112, https://doi.org/10.1016/0379-7112(92)90019-9.

[14] *NFPA 72: Standard for Smoke Control Systems* (2021st ed.). (2021). NFPA .

[15] Francesco, C., & Monica, C. (2018). Fire growth rate strategies in fds. *Journal of Physics: Conference Series*, *1107*(4). https://doi.org/10.1088/1742-6596/1107/4/042007

[16] *3D models for professionals*. TurboSquid. (n.d.). Retrieved March 21, 2023, from https://www.turbosquid.com/

[17] Fryar, C. D., Carroll, M. D., Gu, Q., & Afful, J. (n.d.). *Vital and Health Statistics, Series 3, Number 46*. CDC. Retrieved March 21, 2023, from https://www.cdc.gov/nchs/data/series/sr_03/sr03-046-508.pdf

[18] F. (n.d.). *fds/slread.m at master · firemodels/fds*. GitHub. Retrieved April 10, 2023, from https://github.com/firemodels/fds

[19] *Zaratan HPC Cluster*. (n.d.). UMD High Performance Computing. http://hpcc.umd.edu//hpcc/zaratan.html

[20] F. (n.d.). *fds/bucket_test_1.fds at master · firemodels/fds*. GitHub. https://github.com/firemodels/fds

[21] Andrew F. Siegel, Michael R. Wagner, Chapter 5 - Variability: Dealing with Diversity, Editor(s): Andrew F. Siegel, Michael R. Wagner, Practical Business Statistics (Eighth Edition), Academic Press, 2022, Pages 105-134, ISBN 9780128200254, https://doi.org/10.1016/B978-0-12-820025-4.00005-1.